AD NUMBER

AD857630

NEW LIMITATION CHANGE

TO

Approved for public release, distribution unlimited

FROM

Distribution authorized to U.S. Gov't. agencies and their contractors; Critical Technology; AUG 1969. Other requests shall be referred to Director, Defense Atomic Support Agency, Washington, DC 20305.

AUTHORITY

DNA ltr, 10 Sep 1980

STANFORD RESEARCH INSTITUTE
Menlo Park, California 94025 • U.S.A.

DASA-2324

Special Technical Report 1

August 1969

STATISTICAL ANALYSIS OF LF/VLF COMMUNICATION MODEMS

By: J. K. OMURA

Prepared for:

HEADQUARTERS
DEFENSE ATOMIC SUPPORT AGENCY
WASHINGTON, D.C. 20305

CONTRACT DASA01-68-C-0073

SRI Project 7045

This research has been sponsored by the Defense Atomic Support Agency under NWER Subtask HE 043.

Approved:

R. F. DALY, *Director*
Communication Technology Laboratory

E. J. MOORE, *Executive Director*
Engineering Systems Division

ABSTRACT

This is a two-part technical report that considers the short-time statistical modeling of atmospheric noise at VLF/LF frequencies and applies a new noise model to the performance evaluation of various generic VLF/LF communication modems. In Part One atmospheric noise is examined mainly from a statistical point of view. Next, various statistical models for this type of noise are examined; finally, a new model is developed and compared with available data. In Part Two this noise model is applied to the evaluation of the error probability calculations of various generic VLF/LF modems. Much of Part Two, particularly in regard to a receiver system employing no clipping, is based on classical white Gaussian noise analysis applied to generic modems of interest. When nonlinear clipping is applied, the detailed statistical behavior of atmospheric noise becomes more important, and results depend on the detailed structure of the noise.

CONTENTS

ILLUSTRATIONS

PART ONE

ATMOSPHERIC NOISE MODEL

PART ONE

ATMOSPHERIC NOISE MODEL

I INTRODUCTION

In Part One we develop an analytical model for atmospheric noise that is characterized by its "impulsive" phenomena. Specifically, a new model is developed for radio noise that originates in lightning discharges and propagates large distances to VLF/LF receiving systems. The emphasis here is on development of an accurate short-time, statistical noise model that can be easily applied to the evaluation of the performance of existing VLF/LF communication systems, so that measured noise parameters (such as average power and deviation of the noise voltage envelope) and signal parameters can adequately specify system performance. Noise parameters and estimation of noise parameters are discussed in the final report on this project.[1]* Our goal here is to model the short-time statistical characteristics of atmospheric noise as accurately as is necessary for evaluating the performance of VLF/LF communication systems of interest.

The modeling approach used here is based on the observation that a Gaussian noise model is inappropriate for received atmospheric noise, primarily because Gaussian noise does not have the large dynamic range exhibited by the received noise envelope. Generally, the received atmospheric noise envelope has a log-normal distribution for large envelope values and a Rayleigh distribution for smaller dynamic ranges. Since the envelope of a Gaussian process is Rayleigh distributed, atmospheric noise has a Gaussian behavior only for small dynamic ranges. In a communication system limited by atmospheric noise, the large noise envelopes have the most influence on system performance, and so it is important to characterize accurately the large dynamic range behavior of atmospheric noise.

---

*References are listed at the end of this report.

We next discuss the background for the noise modeling problem. In particular, we examine the physical characteristics of atmospheric noise. Then we discuss existing models for atmospheric noise and introduce the noise model developed in this study. Finally, the properties of this new noise model are examined and compared with available atmospheric noise data.

II PHYSICAL DESCRIPTION OF ATMOSPHERIC NOISE*

A. Introduction

The main source of atmospheric noise at frequencies in the VLF (3-30 kHz) and LF (30-300 kHz) bands is the lightning discharge. Each flash generates a sequence of VLF pulses having certain characteristics. The thunderstorm--as a whole--has a lifetime during which the nature of the lightning flashes that take place and their rate of production may vary. The occurrence of thunderstorms has a climatologically predictable spatial and temporal pattern. Thus the definition of the thunderstorm sources of VLF atmospheric noise may be considered under three divisions: the signals due to a single flash, the sequence of discharges in a single thunderstorm, and the distribution temporally and spatially of the centers of thunderstorm activity over the globe.

After the VLF noise signals have been generated, they are propagated in accordance with the established laws of VLF radio propagation. Thus in order to determine the noise environment at a particular time and locality, three steps are necessary: first, to establish the nature of the noise signals emanating from a typical thunderstorm center; next, to determine the relative activities and the distances of the main thunderstorm centers from the locality being considered at the specified time; and, finally, to introduce the modifications caused by propagation to the noise originating in the various thunderstorm centers.

This chapter summarizes some of the aspects of VLF atmospheric noise specified above. Particular attention is given to source effects. Most of the topics summarized here are considered in much greater detail in Ref. 2.

---

*This chapter was prepared by Dr. E. T. Pierce.

B. The Signals from a Single Lightning Flash

1. The Flash to Earth

The duration of a discharge to earth varies from a few tens of milliseconds to over a second; 400 ms is perhaps a reasonable mean value. The flash is characterized by an initial L stage during which a leader moves downward from the cloud towards the earth. This is succeeded, after contact has been made with the ground, by an intermediate stage characterized by the occurrence of one or more brilliant return (R) strokes. After the last return stroke there is a further gradual flow of current during the final (F) stage. The leader stage of the flash to earth occupies some 50 ms, while 100 ms is a typical duration for the F stage; thus st of the discharge is occupied by the intermediate, R, stage.

Figure 1 illustrates the structure of the VLF noise due to a flash to earth at a distance of 100 km. The field-change records in the figure [(a)] are typical of those obtained using a bandwidth of 1-1000 Hz; these records are dominated by the electrostatic component of the change in field. The records of Type (b) are for a bandwidth of 1-100 kHz. It is easily seen, from comparing records of Type (a) and Type (b), that the main VLF pulses are associated with return strokes (R pulses), but that small L pulses occur during the leader stage while somewhat larger K pulses are present in the intermediate and final stages.

The number of return strokes per flash to earth may vary from one to ten or more; the average is about three to four. The median interval between the strokes is some 50 ms, and the distribution of intervals is skew towards the large-interval end; some 15 percent of the intervals exceed 100 ms, while about 20 percent are less than 30 ms. Figure 2 illustrates the typical amplitude spectrum for an R pulse; the vertical scale applies at a distance of 100 km. Note that the VLF disturbance due to the first return stroke is larger in magnitude and peaks at a higher frequency than that caused by a subsequent return stroke. However, the sizes of both the first and the subsequent R pulses vary

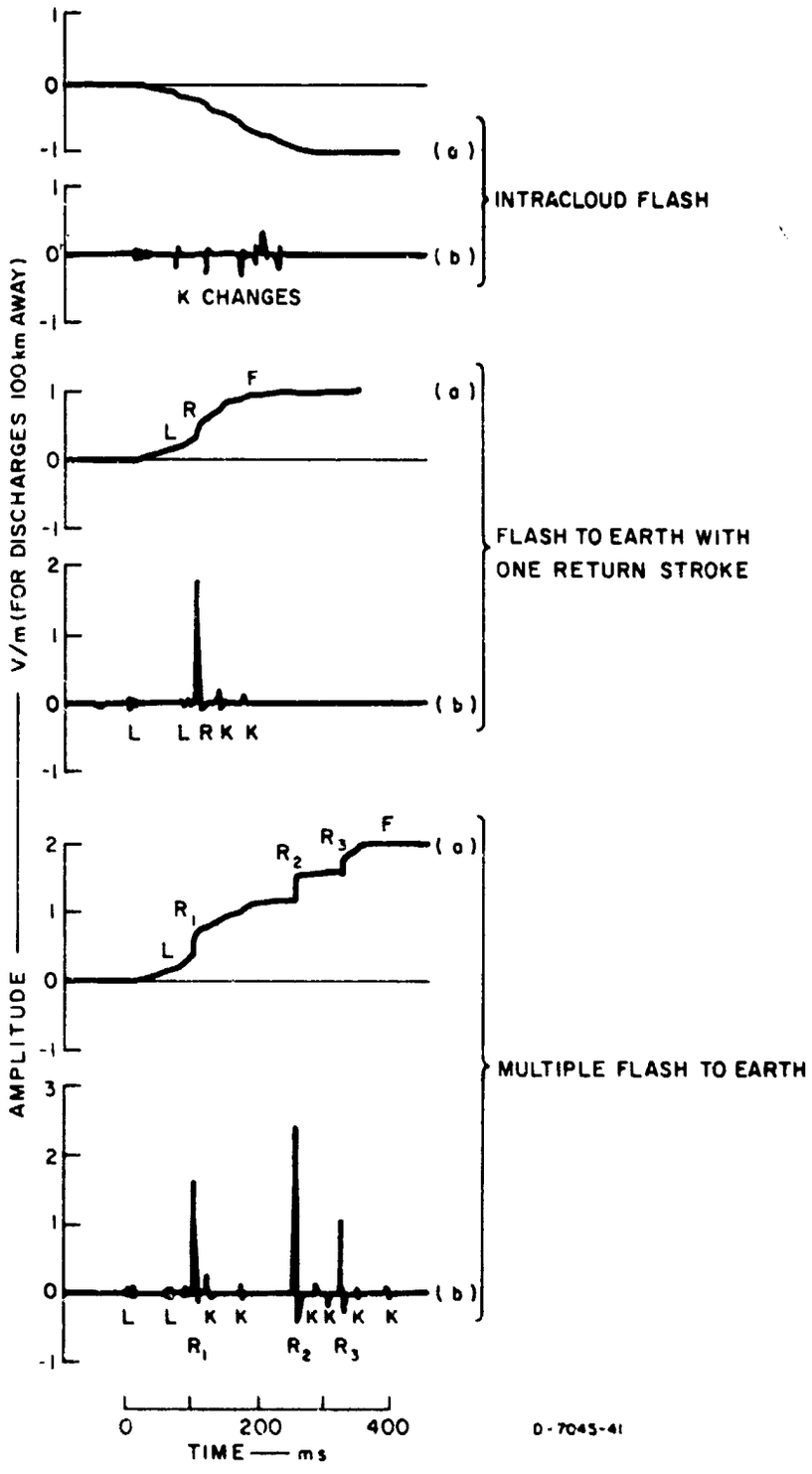

FIGURE 1 FIELD CHANGES AT 100 km DUE TO TYPICAL LIGHTNING DISCHARGES

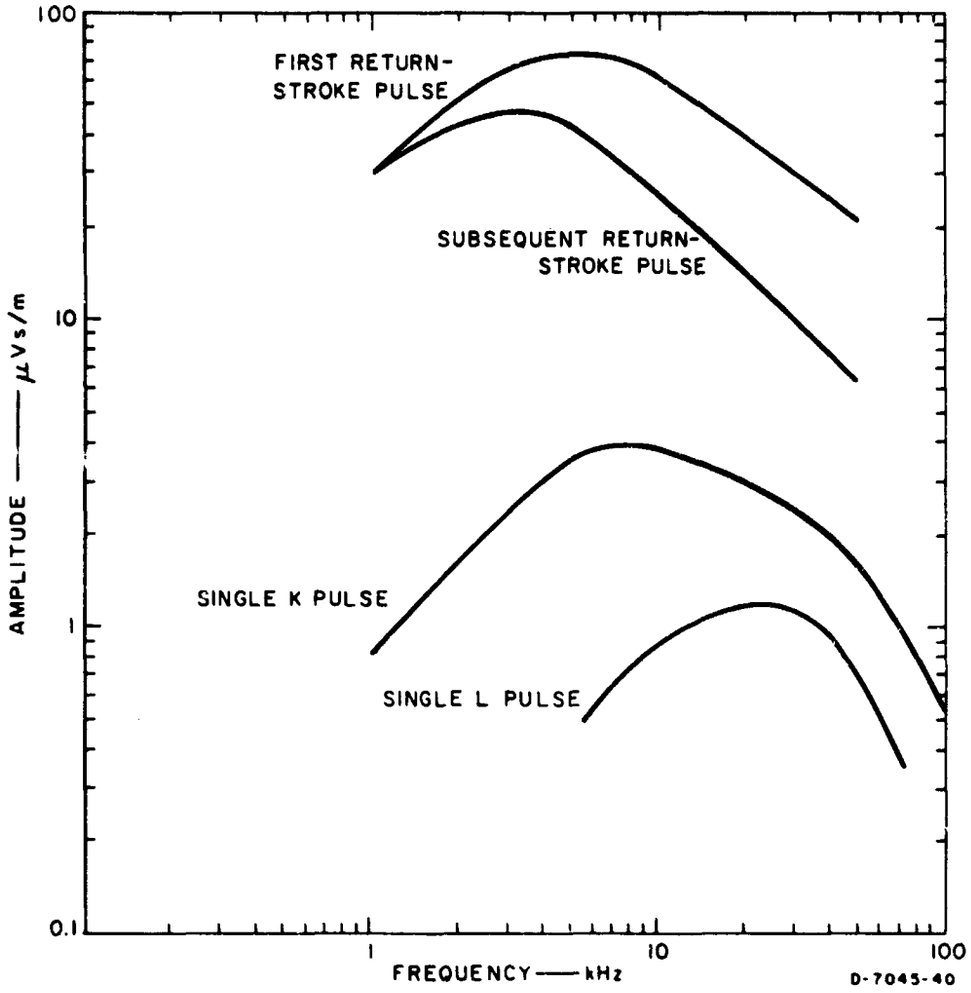

FIGURE 2 COMPARISON OF SPECTRA AT 100 km DUE TO VARIOUS PROCESSES IN A LIGHTNING FLASH

over a wide range; if the amplitudes are expressed in decibels relative to the median, the distribution is normal with a standard deviation of about 6 dB.

The K pulses occur intermittently throughout the intermediate and final stages. The average time interval between the pulses is about 10-15 ms, and the distribution of time intervals is skew towards the large value end. A typical flash to earth produces perhaps 25 K pulses. The spectrum of an average K pulse tends to peak at a rather higher frequency--see Fig. 2--than that of an R pulse, while the

magnitude is perhaps some 10 percent of that for an R pulse. The amplitude distributions for the K and R pulses appear to be similar, both being log-normal with a standard deviation of some 6 dB. Thus, since there are perhaps ten times as many K pulses as R pulses per flash, it is not unusual for the largest K pulse in a discharge to ground to be larger than the smallest R pulse.

Irregular L pulses occur during the L stage of the discharge. Typically two or three pulse trains, each consisting of some 60 L pulses with a total duration of about 3 ms, are produced. The disturbance associated with an individual L pulse is small, and since the L pulses are generated for a time normally less than 10 ms, the L effects can usually be neglected by comparison with the K and R phenomena.

2. The Intracloud Discharge

The structure of the VLF noise from a flash within a thundercloud is much simpler than that of the disturbance associated with a discharge to earth. Intracloud flashes do not generate R pulses, but they produce intermittent K pulses throughout the duration of the discharge. In addition, small irregular pulses are generated in the initial stages of the intracloud flash, but their effect is negligible compared with those of the K pulses.

The durations of flashes to earth and those of intracloud discharges are comparable. Furthermore, the time separation and magnitudes of the K pulses are similar for the two types of flash. Thus, to a first approximation, we may regard the VLF noise due to an intracloud discharge as being identical to the contribution for a flash to earth associated with K pulses.

C. Characteristics of a Thunderstorm

An average thunderstorm has a duration of perhaps 2 hours. During the lifetime of the storm, the flashing rate varies appreciably; the peak rate is about ten discharges per minute and the average some three per minute. Most of the discharges in a storm are of the intracloud or

allied types; typically, some 20 percent of all flashes go to earth, and this proportion increases with an increase in geographical latitude.

D. Climatology of Thunderstorms

It is usually estimated that about 2000 thunderstorms are active at any instant and that the rate of lightning occurrence integrated over the whole surface of the earth is about 100 per second. These figures are exactly compatible with an average flashing rate per storm of three per minute.

There are three especially important global centers of thunderstorm activity: in Southeast Asia, Central Africa, and South America. Each center has its maximum of activity in the local afternoon; this--see Fig. 3--leads to a characteristic global diurnal variation in lightning occurrence. This variation has of course, superimposed seasonal changes.

E. Summary

The procedures for estimating the atmospheric noise at a particular locality and time, due to global lightning, are now clear. We first determine the rate of flashing at each of the main thunderstorm centers from curves such as those of Fig. 3. If for any center the flashing rate is 5r per second, then we have about 4r intracloud flashes and r discharges to earth. Each flash to earth gives--on an average--three to four R pulses, separated by some 50 ms, while all discharges, whether to earth or not, generate about 25 K pulses at intervals of perhaps 10 ms. We may assume the flash occurrence within a main thunderstorm center to be random, since many individual storms will be active simultaneously. Thus at peak activity one of the main thunderstorm centers will be producing about 5r flashes per second, and therefore some 35 R pulses and perhaps 1250 K pulses per second. The bigger R pulses will give the log-normal high-amplitude end often apparent in an experimentally observed amplitude distribution curve; the smaller R pulses and the K pulses will yield the small-amplitude Rayleigh end of the amplitude-distribution curve.

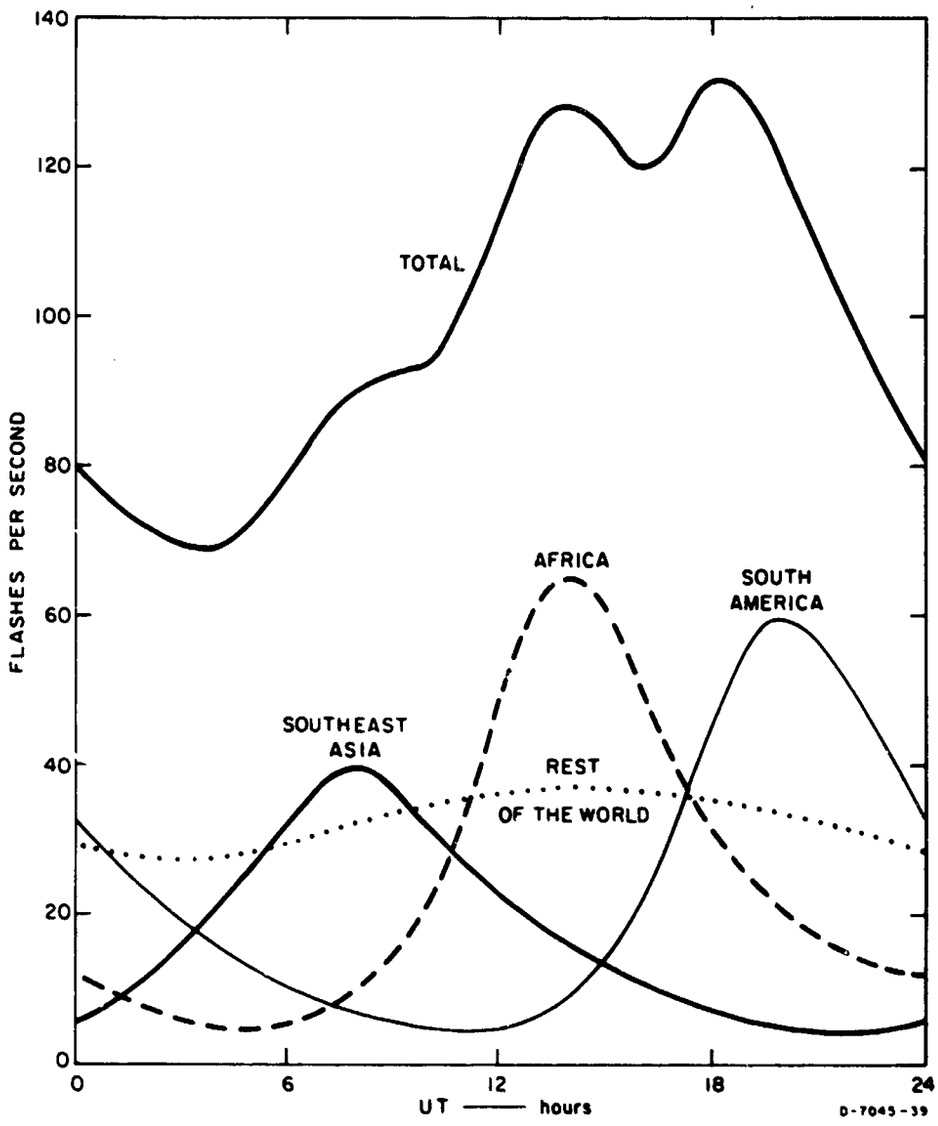

FIGURE 3 DIURNAL VARIATION OF LIGHTNING OCCURRENCES

After the characteristics (amplitude and temporal variations in pulses emitted) of a particular source have been established, the contribution of this source to the noise at the locality being considered can be derived by introducing the appropriate propagational modification to the source disturbance. Integration over all sources then gives the total noise. Note that, if all the significant source centers are very distant or strongly active at intermediate distances, then the received noise will be dominated by a very large incidence of smallish pulses.

Only if the activity is principally due to local storms, or to medium activity at intermediate distances will the incidence of large isolated pulses be significant.

III SUMMARY OF EXISTING MODELS FOR ATMOSPHERIC NOISE

Before a new model for atmospheric noise is described, a brief summary of available models is now presented. Various analytical models for received atmospheric noise have been proposed, usually from one of two points of view. Briefly, the most interesting approach from a physical point of view takes the received noise to be the weighted sum of contributions from individual lightning discharges. Although this approach is physically well justifiable, it has the disadvantage that the resulting models are not analytically tractable. The alternative approach is an empirical method that yields analytical models chosen to fit the measured statistics of the noise. Unfortunately, not only is direct physical support for this procedure lacking, but the existing empirical models suffer from the fact that only the first-order statistics of the noise are considered while the higher-order statistics are neglected.

The models based on the weighted sum of individual lightning discharges are often referred to as filtered-impulse models.[3-6] These physically motivated noise models have the typical form

$$a(t) = \sum_i a_i \, p(t - t_i) \quad , \tag{1}$$

where the $\{a_i\}$ are independent, identically distributed random variables whose distribution is deduced from lightning discharge statistics and propagation consideration; $p(t)$ gives the form of the noise pulse resulting from an individual lightning stroke, as shaped by the front-end filter of the receiver; and the $\{t_i\}$ are the occurrence times of the individual lightning strokes. Under the assumption that each individual lightning stroke is independent of others, various results[4-6] have been obtained on the first-order statistics of the noise. In particular, probability distributions are typically derived for these models, since this distribution has been measured quite extensively.[4,7-10] Although the analytical results due to different assumptions on $p(t)$, $\{t_i\}$, and

$\{a_i\}$ result in varying agreement with measured data, the resulting analytical probability distributions are quite complicated and difficult to use in performance calculations. Indeed, the resulting probability distributions often cannot be written in closed form except for some limiting cases. Also the assumption of independence between individual lightning strokes which is crucial to the solution of the first-order statistics of a(t) does not appear to be true at VLF.[7] This means that any second-order (or higher-order) statistic would not be accurately modeled by these noise models. Conceivably, the independent assumption might be eliminated by introducing dependence in the filtered-impulse model, as was done by Furutsu and Ishida,[4] who considered the case of Poisson-Poisson noise. Although this interdependence model has not yet been demonstrated to yield the distribution of interlevel-crossing intervals observed by Watt and Maxwell at VLF,[7] it is already too difficult to handle for performance calculations.

Noise models based on the empirical method generally consist of mathematical expressions constructed to fit the measured data on the first-order statistics of the envelope of the received noise. These are models of the envelope distribution and not of the whole noise process as is the case with filtered-impulse models. Not only are these empirical models not physically motivated, but by their construction they are good for only first-order calculations. Although they are relatively simple to handle for first-order calculations, their range of application is limited.

Ibukun[10] presents a good summary of various empirical models that have been proposed. Several other workers[11-13] have had some success in finding physical justification for empirical models. Perhaps the most important of these models, because of its simplicity and its closeness of fit to measured data, is the model that takes the envelope of the received atmospheric noise to be Rayleigh distributed at low values of the envelope and log-normally distributed at high values. Beckmann[13] has given a good physical argument which supports this model, particularly in the situation where there is little local thunderstorm activity.

Several workers[10,13,14] have proposed models similar to that considered by Beckmann, although they differ in regard to how much of the two distributions should be combined to result in the best model.

One of the most important recent atmospheric noise models is due to Hall[15] and is called the generalized "t" model. This modeling effort takes a point of view different than those leading to either the filtered-impulse models or the empirical models discussed above. The generalized "t" model describes the received atmospheric noise as

$$a(t) = b(t)n(t) \quad , \tag{2}$$

where n(t) is a narrow-band Gaussian process, and b(t) is a slowly varying process, independent of n(t). This model gives some physical support to perhaps the simplest of the empirical models,[10,16] which has probability $P_o(V)$ that the noise envelope exceeds the value V,

$$P_o(V) = \left[1 + \left(\frac{\alpha V}{\bar{V}}\right)^r\right]^{-1} \quad , \tag{3}$$

where $\bar{V}$ is the average value of the envelope and α and r are two parameters to be chosen. This empirical model is also the same as the model studied by Mertz.[17,18] Not only do the first-order statistics of Hall's generalized "t" model agree closely with this class of empirical models, but it has the advantage over empirical models in that it can be specified to give a good fit to the higher-order statistics of the noise also.

Using the approach of Hall, we next develop an atmospheric noise model that is perhaps mathematically simpler than Hall's generalized "t" model and yet has as good an agreement with first- and second-order statistical data as the generalized "t."

IV LOG-NORMAL NOISE MODEL

A. Introduction

Turning attention now to the problem of developing a model for received atmospheric noise, we note that this noise is always observed through the passband of some receiver filter. Now, if the receiver is sufficiently narrow-band, the noise at the receiver output can reasonably be assumed to be modeled well as a Gaussian process. This follows from the fact that narrow-band filtered noise is the sum of contributions from many independent lightning discharges, none of which is dominant at the filter output. Experimental data indicate, however, that the bandwidth required to achieve this condition at VLF is less than 50 Hz, so a Gaussian assumption is not always physically viable at VHF. The goal of the model development here is the formulation of an analytical model that is both an accurate description of the received noise and suitable for application to the calculation of VLF/LF communication system performance. As far as the communication problem is concerned, it appears necessary to model the atmospheric noise prior to any receiver operations, so a Gaussian assumption is not always justified. This is particularly true when nonlinear operations are performed by the receivers.

The modeling problem can be simplified by noting that for communication application the receiver bandwidths are substantially smaller than the band center frequency. This fact enables the received atmospheric noise to be regarded as a narrow-band random process. This is always satisfied for communication problems and is not nearly as strong an assumption as a Gaussian assumption. Almost all the available experimental data[4,7-10] have been obtained in narrow-band conditions.

Measured data on atmospheric noise indicate that this noise has a Gaussian behavior at low amplitudes and a log-normally distributed envelope for large amplitudes. Beckmann explains this fact by noting that measured atmospheric noise usually consists of the effects of many lightning discharges around the world. When no single discharge dominates at any instant of time, then, applying the central limit theorem,

we should expect a Gaussian behavior. On the other hand, when a particular individual discharge dominates, the measured amplitude has the statistical characteristics of the individual discharge which is essentially log-normal in character. Since the larger amplitudes have the greater influence on the performance of any communication system, our model emphasizes the log-normal characteristic of atmospheric noise. In particular, we model atmospheric noise as a narrow-band process with a log-normal envelope with the form

$$a(t) = A\, e^{n(t)} \sin\left[\omega_o t + \theta(t)\right] \quad , \tag{4}$$

where $n(t)$ is a stationary Gaussian process with zero mean and autocorrelation given by

$$R_n(\tau) = \overline{n(t)n(t+\tau)} \quad ,^{*} \tag{5}$$

A is a constant (to be determined from noise power estimates), and $\theta(t)$ is a random phase process independent of the Gaussian process $n(t)$.

To illustrate the behavior of the envelope of this model, consider Fig. 4. In Fig. 4(a), we plot a sample Gaussian process $n(t)$. In Figs. 4(b), (c), and (d) we plot $e^{n(t)}$ to show how the envelope of this model behaves for typical values of V_d (voltage deviation, the ratio of the root-mean-square voltage to the average voltage of the noise envelope). By proper adjustment of parameters, this model reflects the impulsive nature of atmospheric noise that has passed through a receiver front-end filter.

In our model given by Eq. (4) we have not yet specified the behavior of the phase process $\theta(t)$. Measurements of the instantaneous frequency distribution for atmospheric noise show that it is similar to the frequency distribution of narrow-band Gaussian noise. Hence, even

---

*Here $\bar{x}$ is the expected value of x.

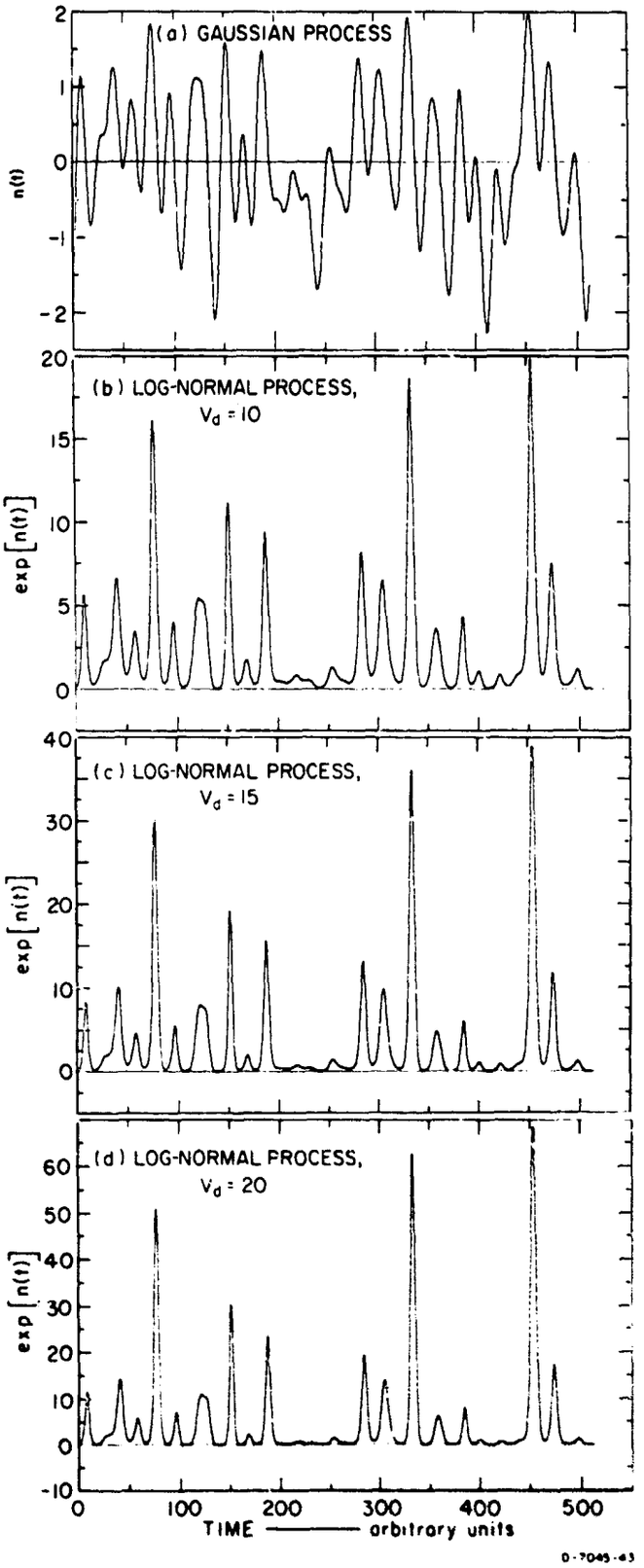

FIGURE 4 ENVELOPE MODEL FOR GAUSSIAN AND LOG - NORMAL PROCESSES

though the envelope behavior of atmospheric noise and that of Gaussian noise differ considerably for large envelope values, the phase and frequency behavior are quite similar. We therefore assume that $\theta(t)$ behaves like the phase of narrow-band Gaussian processes. This means that at any given instant t_o, the phase $\theta(t_o)$ is a random variable that is uniformly distributed over $[0, 2\pi]$ and is independent of the envelope.

B. Properties of the Log-Normal Model

The log-normal narrow-band noise model for atmospheric noise is given by

$$a(t) = A\, e^{n(t)} \sin\left[\omega_o t + \theta(t)\right] \quad . \tag{6}$$

Assuming stationarity we note that the envelope of this noise,

$$E(t) = A\, e^{n(t)} \quad , \tag{7}$$

has autocorrelation given by

$$\begin{aligned} R_E(\tau) &= \overline{E(t)E(t+\tau)} \\ &= A^2\, \overline{e^{n(t)+n(t+\tau)}} \\ &= A^2\, e^{\left[\sigma_n^2 + R_n(\tau)\right]} \quad , \end{aligned} \tag{8}$$

where $\sigma_n^2 = R_n(0)$ is the variance of $n(t)$.

The average power of the noise model is given by

$$\begin{aligned} R_a(0) &= \overline{a(t)a(t+\tau)} \\ &= A^2\, \overline{e^{2n(t)} \sin^2\left[\omega_o t + \theta(t)\right]} \end{aligned} \tag{9}$$

$$R_a(0) = A^2 \, \overline{e^{2n(t)}} \; \overline{\sin^2\left[\omega_o t + \theta(t)\right]}$$

$$= A^2 \, e^{2\sigma_n^2} \times \frac{1}{2}$$

$$= \frac{A^2}{2} e^{2\sigma_n^2} \quad . \tag{10}$$

If we assume that the noise has an approximately flat energy distribution of N_o watts per hertz across the receiver front-end bandwidth of W Hz, then we have the relation

$$N_o W = \frac{A^2}{2} e^{2\sigma_n^2} \quad . \tag{11}$$

Consider the average and rms voltages of the envelope. The average is

$$E_{ave} = \overline{E(t)} = A \, \overline{e^{n(t)}}$$

$$= A \, e^{\frac{1}{2}\sigma_n^2} \quad , \tag{12}$$

and the rms envelope voltage is

$$E_{rms} = \sqrt{\overline{E^2(t)}} = \left\{ A^2 \, \overline{e^{2n(t)}} \right\}^{\frac{1}{2}}$$

$$= A \, e^{\sigma_n^2} \quad . \tag{13}$$

The voltage deviation, V_d, is defined as

$$V_d = 20 \log_{10} \left(\frac{E_{rms}}{E_{ave}} \right)$$

$$= 20 \log_{10} \left(e^{\frac{1}{2}\sigma_n^2} \right) \tag{14}$$

$$= 10\sigma_n^2 \log_{10} e \quad .$$

Knowledge of V_d gives us the value of σ_n^2. Similarly, knowing V_d (hence σ_n^2) and the noise power density, N_o, we can find the parameter A. Values of V_d and of F_a, which is directly related to N_o, are estimated in CCIR reports.[19]

We have now related parameters of our noise model directly to the measurement parameters that are typically used in world CCIR maps. Our next task is to show how well this noise model agrees with available statistical data on atmospheric noise. The measurements required to check the validity of the model fall into two categories.

The first of these categories, and the one for which the greatest amount of experimental data is available, is concerned with the first-order statistics of the random process. The particular measurements in this category that have been reported in the literature are measurements of the probability distribution of the envelope of the received noise,[4,7-10] and measurements of the average number of level crossings per unit time of a fixed level by the envelope of the received noise.[7,8] This latter calculation has not been carried out for any of the empirical models discussed earlier, although Nakai[20] has obtained numerical results in agreement with the experimental data of Watt and Maxwell for a filtered-impulse model in which the noise pulses occur in a Poisson manner. Hall[15] has also obtained good agreement with experimental data with his generalized "t" noise model. In fact, he has also shown good agreement with second-order experimental data which we discuss next.

The second category of measured data, and the one where far fewer data are available, is concerned with the second- and higher-order statistics of the random process. The particular measurements that have been reported in this category are measurements of the probability distribution of the time interval between crossings of a specified level by the envelope of the noise.[7] While available experimental data are sparse, being restricted to a few measurements at VLF, it is also true that the analytical derivation of these statistics is complicated, requiring machine computation in the general case. Hall was able to compare a limiting case of his generalized "t" noise model with second-order data

and demonstrated reasonable agreement between his model and the available data. We use similar approximations to demonstrate agreement of our log-normal model with higher-order data.

1. First-Order Statistics

The envelope of our log-normal narrow-band atmospheric noise model is given by

$$E(t) = A\, e^{n(t)} \quad . \tag{15}$$

We now derive some first-order statistical properties of this envelope and compare them with available data. At any instant of time,

$$E = A\, e^{n} \tag{16}$$

is a random variable, where n is a zero-mean, Gaussian, random variable with variance σ_n^2. The probability distribution of E is

$$\begin{aligned} P(V) &= P_r\{E \le V\} \\ &= P_r\{A\, e^{n} \le V\} \\ &= P_r\{e^{n} \le (V/A)\} \\ &= P_r\{n \le \log_e(V/A)\} \\ &= \psi\left(\frac{\log_e(V/A)}{\sqrt{\sigma_n^2}}\right) \quad . \end{aligned} \tag{17}$$

where

$P_r\{A\}$ is the probability of the event A, and

$$\psi(\alpha) = \int_{-\infty}^{\alpha} \frac{1}{\sqrt{2\pi}}\, e^{-\frac{x^2}{2}}\, dx \tag{18}$$

is the well-known distribution of a zero-mean, unit-variance Gaussian random variable.[21] Defining

$$P_o(V) = 1 - P(V)$$
$$= 1 - \psi\left(\frac{\log_e(V/A)}{\sqrt{\sigma_n^2}}\right) \quad , \tag{19}$$

we compare this probability distribution of the envelope derived from our model with measured data on the distribution of the envelope of atmospheric noise. Figures 5 and 6 compare the above distribution with experimental data for various receiver parameters. Note that

$$V_{ave} = E_{ave} = A\, e^{\frac{1}{2}\sigma_n^2} \quad . \tag{20}$$

Hence

$$P_o(V) = \psi\left(\frac{\log_e\left(V/V_{ave}\right) - \frac{1}{2}\,\sigma_n^2}{\sqrt{\sigma_n^2}}\right) \tag{21}$$

and σ_n^2 is the only free parameter in the figures.

The plotted results are reasonably self-explanatory, showing good agreement between the model and the measured data. Again, we point out that our intention is to model the large envelope variations more accurately than previously, since these variations have the most influence on communication system performance. Consequently, our model matches the experimental data more accurately for larger values of the envelope.

We next consider another experimentally measured first-order statistical property, the average frequency of envelope level crossings. Consider the envelope process and the level B indicated in Fig. 7(a). We are concerned with the average number of times E(t) crosses the level B in T seconds. This is equivalent to asking for the average number of times the Gaussian process n(t) crosses the level

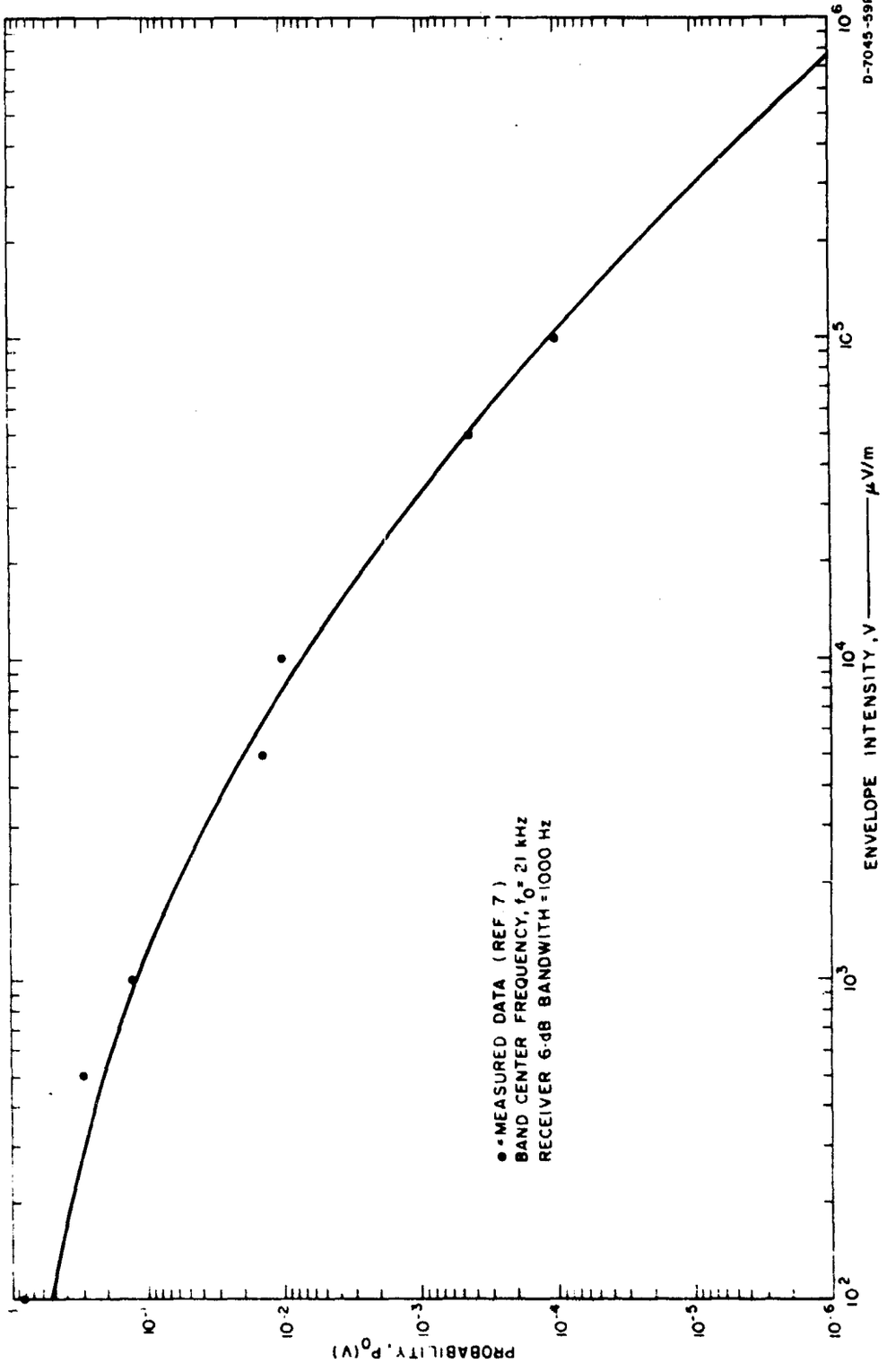

FIGURE 5 PROBABILITY DISTRIBUTION OF THE ENVELOPE FOR AVERAGE VOLTAGE ≅ 800 μV/m

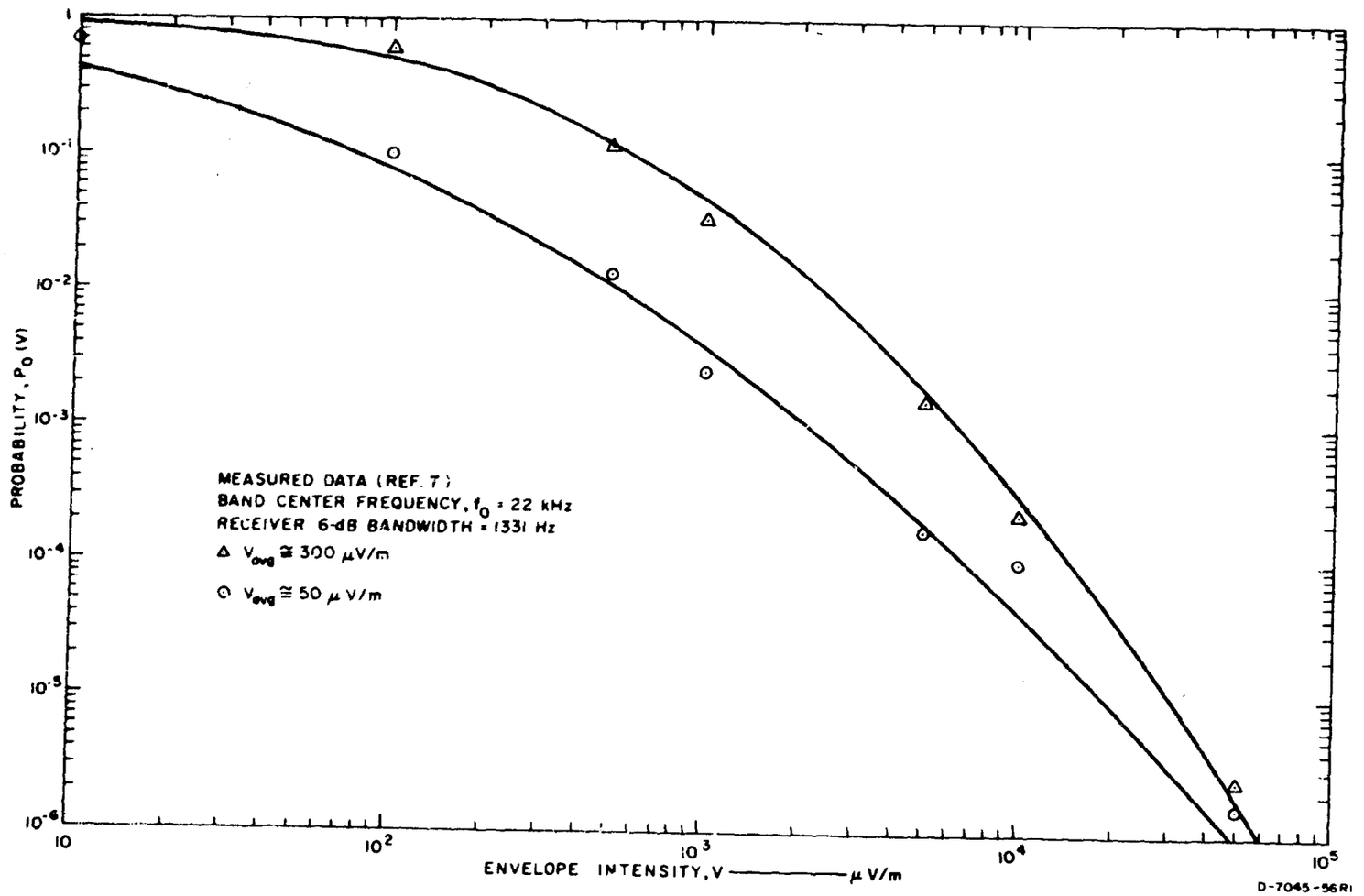

FIGURE 6 PROBABILITY DISTRIBUTION OF THE ENVELOPE FOR AVERAGE VOLTAGE ≅ 300 AND 50 μV/m

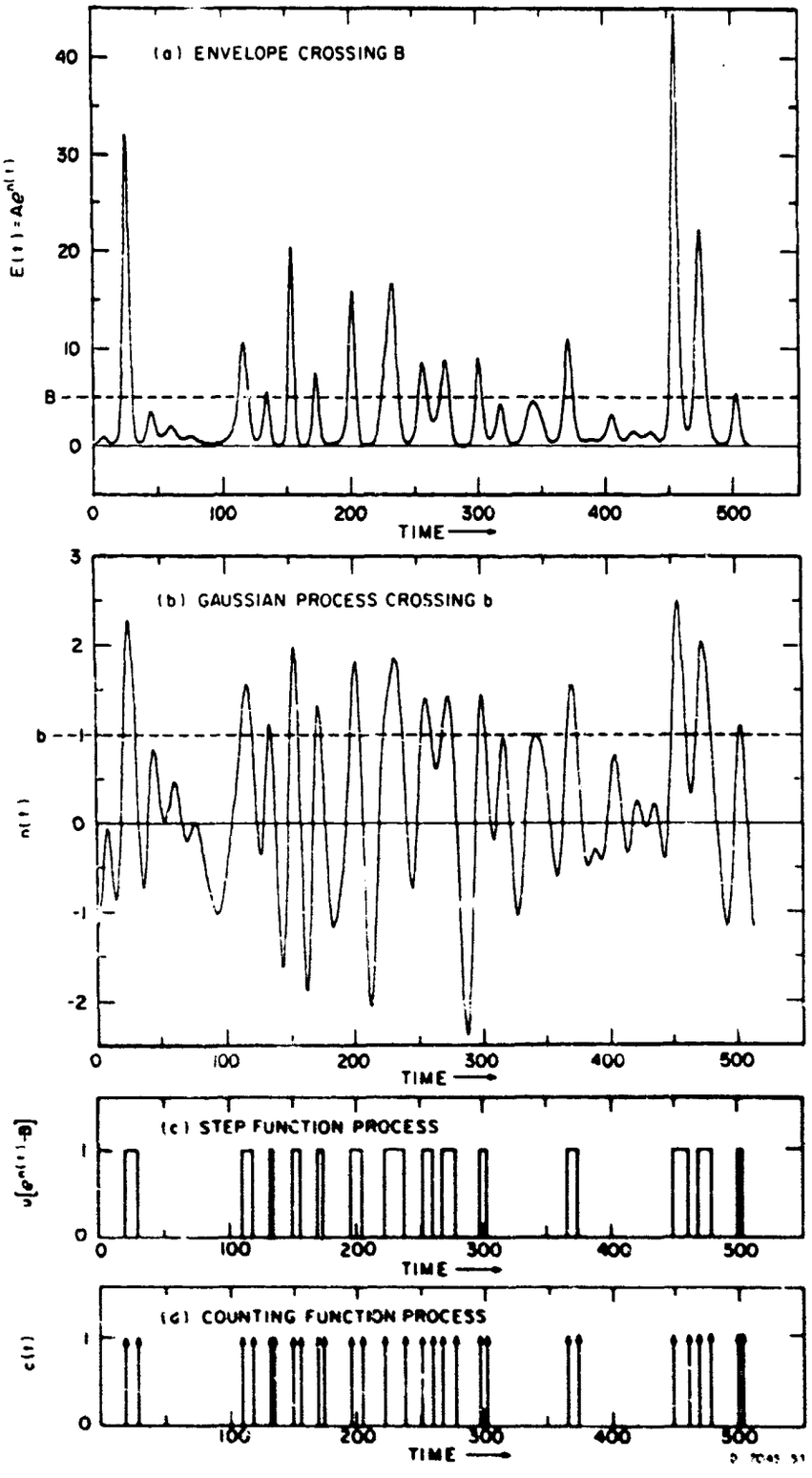

FIGURE 7 ENVELOPE LEVEL CROSSINGS AND ASSOCIATED STEP AND COUNTING FUNCTION PROCESSES

$$b = \log_e(B/A) \quad . \tag{22}$$

In Fig. 7(b) the equivalent Gaussian process crossing level b is shown.

We define a counting function

$$\begin{aligned} c(t) &= \left|\dot{u}[n(t) - b]\right| \\ &= \left|\dot{u}[E(t) - B]\right| \quad , \end{aligned} \tag{23}$$

which gives a unit impulse each time [n(t) = b or E(t) = B] the level b is crossed by n(t). Since we want to count the number of crossings in a time interval of length T, the count is given by

$$\begin{aligned} N_B(T) &= \int_0^T c(t)\, dt \\ &= \int_0^T \left|\dot{u}[n(t) - b]\right| dt \quad . \end{aligned} \tag{24}$$

Using the well-known relationship

$$\frac{d}{dt}\{f[g(t)]\} = \frac{df(g)}{dg} \cdot \frac{dg}{dt} \quad , \tag{25}$$

we get

$$N_B(T) = \int_0^T \delta[n(t) - b]\left|\dot{n}(t)\right| dt \quad . \tag{26}$$

Since we have a stationary Gaussian random variable, n(t) and $\dot{n}(t)$ are statistically independent. This follows from the relation

$$\begin{aligned} \overline{n(t)\dot{n}(t)} &= \frac{1}{2}\overline{\frac{d}{dt}\, n^2(t)} \\ &= \frac{1}{2}\frac{d}{dt}\overline{n^2(t)} \\ &= 0 \quad . \end{aligned} \tag{27}$$

Hence,

$$\overline{N_B(T)} = \overline{\delta[n(t) - b]}\,\overline{|\dot{n}(t)|}\,T \quad . \tag{28}$$

The random variable n(t) has a density function

$$p_n(\alpha) = \frac{1}{\sqrt{2\pi\sigma_n^2}} \exp\left\{-\frac{\alpha^2}{2\sigma_n^2}\right\} \tag{29}$$

so

$$\begin{aligned}\overline{\delta(n - b)} &= \int_{-\infty}^{\infty} \delta(\alpha - b)\, p_n(\alpha)\, d\alpha \\ &= p_n(b) \\ &= \frac{1}{\sqrt{2\pi\sigma_n^2}} \exp\left\{-\frac{b^2}{2\sigma_n^2}\right\} \quad .\end{aligned} \tag{30}$$

The probability density of $\dot{n}(t)$ is found by noting that the derivative is a linear operation and that linear operations on a Gaussian process result in another Gaussian process. Thus $\dot{n}(t)$ is a Gaussian random variable with zero mean and variance determined as follows:

$$R(\tau) = \overline{n(t)n(t + \tau)} \tag{31}$$

so

$$\begin{aligned}\dot{R}(\tau) &= \frac{d}{d\tau} R(\tau) \\ &= \overline{n(t)\dot{n}(t + \tau)} \quad .\end{aligned} \tag{32}$$

By stationarity we have

$$\dot{R}(\tau) \quad \overline{n(t - \tau)\dot{n}(t)} \quad , \tag{33}$$

so

$$\ddot{R}(\tau) = \frac{d}{d\tau}\dot{R}(\tau)$$

$$= -\overline{\dot{n}(t-\tau)\dot{n}(t)} \quad . \tag{34}$$

Hence

$$\ddot{R}(0) = -\overline{[\dot{n}(t)]^2} \quad , \tag{35}$$

and the probability density of $\dot{n}(t)$ is

$$p_{\dot{n}}(\alpha) = \frac{1}{\sqrt{2\pi\left[-\ddot{R}_n(0)\right]}} \exp\left\{-\frac{\alpha^2}{2\left[-\ddot{R}_n(0)\right]}\right\} \quad . \tag{36}$$

The term $\overline{|\dot{n}(t)|}$ is given by

$$\overline{|\dot{n}(t)|} = 2\int_0^\infty \alpha\, p_{\dot{n}}(\alpha)\, d\alpha$$

$$= \int_0^\infty \frac{2\alpha}{\sqrt{2\pi\left[-\ddot{R}_n(0)\right]}} \exp\left\{-\frac{\alpha^2}{2\left[-\ddot{R}_n(0)\right]}\right\} d\alpha \quad . \tag{37}$$

Since $\ddot{R}_n(0)$ is related to how rapidly the envelope process goes through changes, the quantity $\overline{|\dot{n}(t)|}$ depends on higher-order statistics of the envelope process.

Combining Eqs. (28) and (30) we find that the average number of times the envelope of our noise model crosses the level B in T seconds is given by

$$\overline{N_B(T)} = \frac{\overline{|\dot{n}|}\,T}{\sqrt{2\pi\sigma_n^2}} \exp\left\{-\frac{\left[\log_e(B/A)\right]^2}{2\sigma_n^2}\right\} \quad . \tag{38}$$

For the special case of T = 1, we have

$$\overline{N_B(1)} = \frac{\overline{|\dot{n}|}}{\sqrt{2\pi\sigma_n^2}} \exp\left\{-\frac{\left[\log_e(B/A)\right]^2}{2\sigma_n^2}\right\} \quad . \tag{39}$$

Figure 8 compares this average level crossing with experimental data. It shows a basic agreement of the results derived by using our log-normal model with measured level-crossing results. Again, we note that the agreement is somewhat better for the larger values of the envelope intensity. The significance of this agreement is, of course, that it is further verification of the applicability of the model as far as the first-order statistics of the noise envelope are concerned. From a physical point of view, this agreement increases confidence in the log-normal narrow-band noise model, since it indicates that on the average the envelope of the received noise is accurately modeled. To complete the verification of the applicability of this noise model for atmospheric noise, it remains to investigate the manner in which these variations occur with time. This is, of course, a function of the second- and higher-order statistics of the noise, which is the next topic of discussion.

2. Higher-Order Statistics

Completion of the verification of the applicability of the narrow-band log-normal process to received atmospheric noise requires investigation into the higher-order statistics of the noise. Although the average rate of level crossings of the envelope of our model generally agrees with observed atmospheric noise, we must yet verify that the higher-order statistics of the model can be so chosen that the relationship between the noise process at various distinct times, as predicted by the model, is consistent with measured results. As mentioned earlier, the available experimental data[7] that are dependent on the higher-order statistics of the noise consist of measurements of the probability distribution function of the interval between successive crossings of a fixed level by the envelope of the noise. Inspection of these data indicates that at VLF the noise pulses do not in general occur in a Poisson fashion but rather that received noise pulses are usually statistically dependent on preceding ones. Generally, calculation of the probability distribution of the interlevel-crossing time interval is difficult, requiring numerical techniques to obtain even an

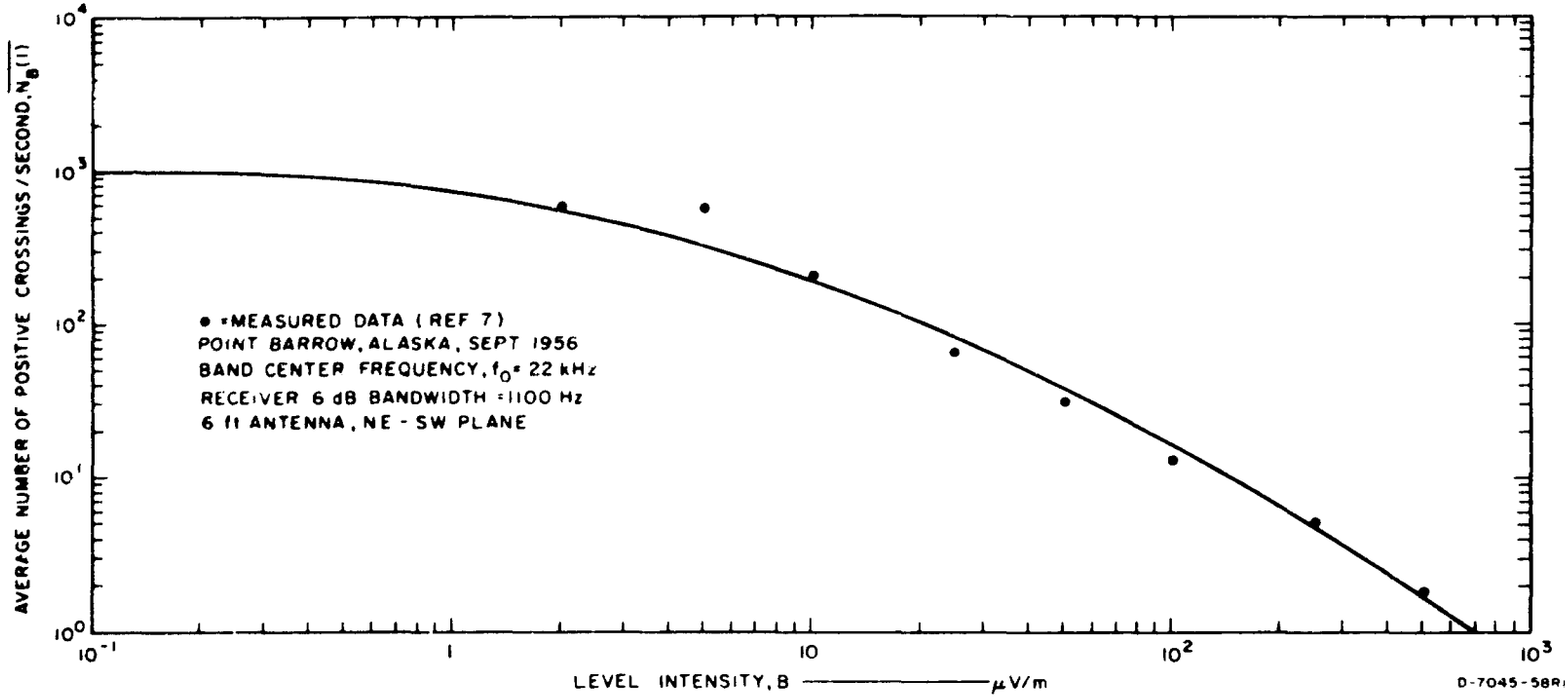

FIGURE 8 AVERAGE NUMBER OF TIMES ENVELOPE CROSSES LEVEL B

approximate solution.[22-24] This is true even for the simplest case of Gaussian processes, which is the only case that has been treated in any detail in the literature.[23,24] Even in the Gaussian case, the problem is further restricted by consideration of Markov processes and a few other specific spectra. Therefore, we will not attempt to find an exact solution for the process of interest here but will resort to simplifying assumptions in order to obtain an approximate solution.

Consider the envelope, E(t), crossing some level B, and let T be defined as the interval between a down-crossing at the level B and the next up-crossing of the same level. (This is the statistical data measured by Watt and Maxwell.[7]) The probability that T exceeds T_o is given by

$$\begin{aligned} P_o(T_o) &= P_r\{T > T_o\} \\ &= P_r\{E(t) \le B, t\in[0,T_o] \mid E(0-) > B, E(0+) < B\} \\ &= \frac{P_r\{E(t) \le B, t\in[0,T_o]; E(0-) > B, E(0+) < B\}}{P_r\{E(0-) > B, E(0+) < B\}} , \end{aligned} \tag{40}$$

where E(0+) is the value of E(t) at a small increment of time after t = 0, and E(0-) is the corresponding value at a small increment of time before t = 0.

At this point, we make several simplifying assumptions by considering N time samples of the envelope process and using these time samples to represent the process. Taking

$$t_o, t_1, \ldots, t_N \tag{41}$$

as the N + 1 time samples, we approximate the desired probability by

$$P_o(T_o) \cong \frac{P_r\{E(t_1) \le B, E(t_2) \le B, \ldots, E(t_N) \le B, E(t_o) > B\}}{P_r\{E(t_o) > B, E(t_1) \le B\}} . \tag{42}$$

Recall that our envelope process

$$E(t) = A\, e^{n(t)} \tag{43}$$

is band-limited to W, so in T_o seconds there are approximately

$$N = 2W\, T_o \tag{44}$$

independent samples. Taking samples to be independent, we then have

$$\begin{aligned} P_o(T_o) &\cong \frac{P_r\{E(t_o) > B\} \prod_{k=1}^{N} P_r\{E(t_k) \le B\}}{P_r\{E(t_o) > B\} P_r\{E(t_1) \le B\}} \\ &\cong \prod_{k=2}^{N} P_r\{E(t_k) \le B\} \quad . \end{aligned} \tag{45}$$

From Eq. (17) we have

$$P_r\{E(t_k) \le B\} = \psi\left(\frac{\log_e(B/A)}{\sqrt{\sigma_n^2}}\right) \quad ; \tag{46}$$

therefore

$$P_o(T_o) \cong \left[\psi\left(\frac{\log_e(B/A)}{\sqrt{\sigma_n^2}}\right)\right]^{(2WT_o - 1)} \quad . \tag{47}$$

In Fig. 9 we plot this distribution along with data taken from Watt and Maxwell. The assumption of independent samples neglects certain dependencies between adjacent level crossings. This assumption was necessary to obtain a simple closed-form expression for $P_o(T_o)$ and is not necessarily a limitation of the log-normal model. Indeed, by appropriately choosing $R_n(\tau)$, a more accurate agreement with data is possible, and only our ability to compute $P_o(T_o)$ in a convenient form is limited. In a more general case, for example, we would have

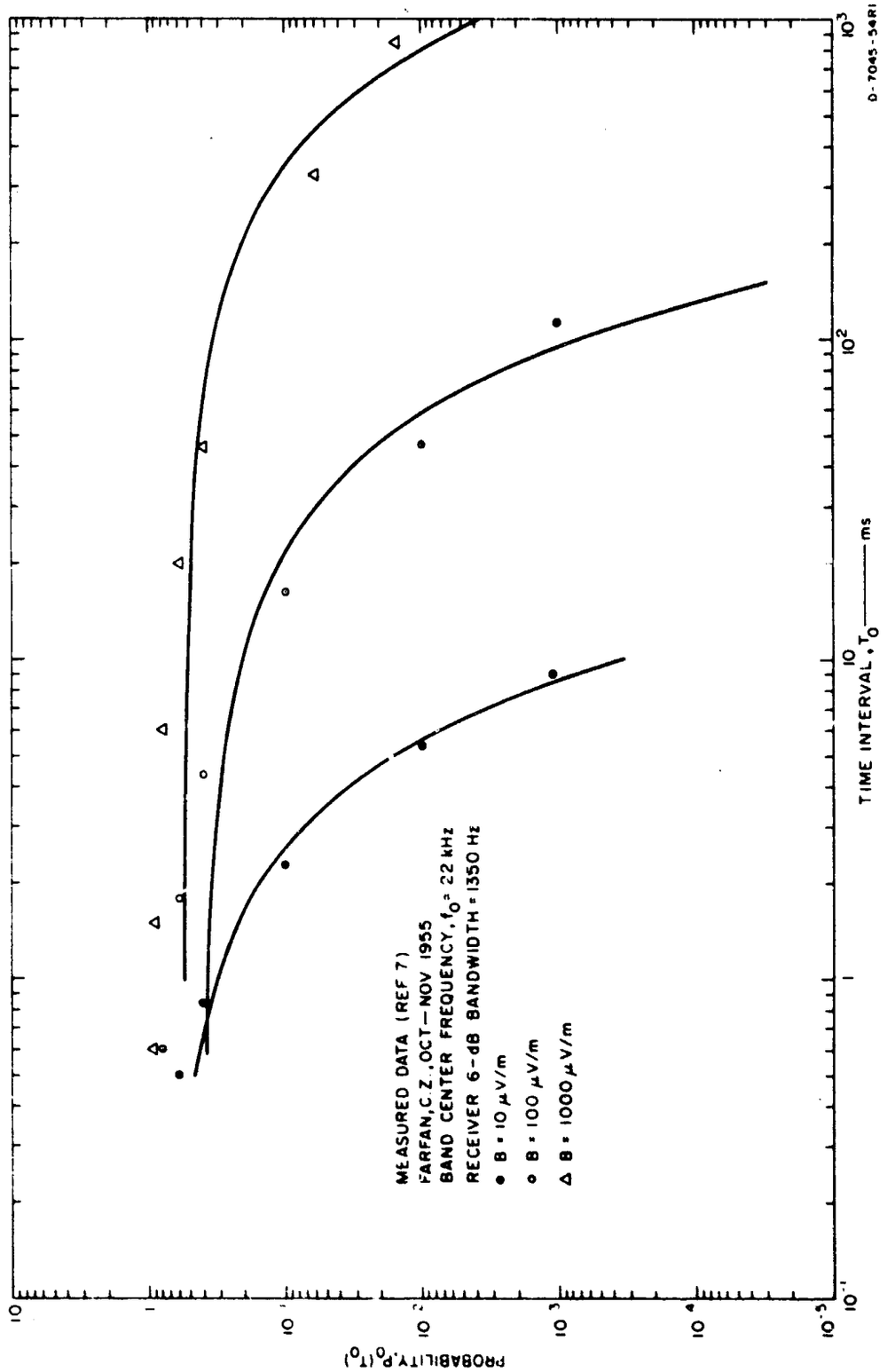

FIGURE 9 PROBABILITY DISTRIBUTION OF TIME BETWEEN CROSSINGS OF LEVEL B

$$P_o\ T_o \cong \frac{\int_b^\infty \int_{-\infty}^b \cdots \int_{-\infty}^b \frac{1}{\{2\pi|\underline{K}|\}^{N/2}} \exp\left\{-\underline{\alpha}'\underline{K}^{-1}\underline{\alpha}\right\} d\underline{\alpha}}{\int_{-\infty}^b \int_b^\infty \frac{1}{2\pi\left[\sigma_n^2\left(\sigma_n^2 - R_n\left(t_1 - t_o\right)\right)\right]^{\frac{1}{2}}} \exp\left\{-\frac{\left(\alpha_1^2+\alpha_2^2\right)\sigma_n^2 - 2\alpha_1\alpha_2 R_n\left(t_1-t_o\right)}{2\sigma_n^2\left[\sigma_n^2 - R_n\left(t_1-t_o\right)\right]}\right\} d\alpha_1 d\alpha_2} \tag{48}$$

where

$$b = \log_e(B/A)$$

and

$$\underline{K} = \left\{R_n\left(t_i - \tau_j\right)\right\}_{i,j} \text{ is an } (N+1)\text{-dimensional covariance matrix.}$$

C. Conclusion

We conclude that the log-normal atmospheric noise model gives good agreement with measured data, especially for larger values of the envelope. This applies for the first-order statistics as well as the higher-order ones. This model is also relatively easy to handle analytically and thus is useful for calculating the performance of communication systems.

PART TWO

ERROR PROBABILITIES OF GENERIC VLF/LF MODEMS

PART TWO

ERROR PROBABILITIES OF GENERIC VLF/LF MODEMS

I INTRODUCTION

In this part we discuss the performance of various generic VLF/LF communication systems of interest. The usual performance measure of probability of error will be expressed in terms of the signal strength and noise parameters at the receiver's antenna. As we have discussed in Part One, the noise has an impulsive non-Gaussian behavior which we have modeled. The receiving systems we will consider can also have nonlinear clipping which, together with the non-Gaussian noise behavior, makes computation of the error probabilities difficult if not impossible without some assumptions. Our assumptions are discussed and justified as they arise in the development of error probability expressions. We first discuss the noise model, the signal characteristics, and the receiving system models before carrying out the development of the error probability expressions. The VLF/LF communication systems we consider include binary frequency shift keying (FSK), phase shift keying (PSK), and minimum shift keying (MSK), all operating in a coherent mode. On-off keying (CW) and noncoherent FSK are also considered, as well as differential phase shift keying (DPSK). Two signaling schemes that use long sequences of MSK pulses (chips) are also discussed.

II PROPERTIES OF THE NOISE MODEL

At VLF and LF, the dominant noise source is generally atmospherics. Local activity often produces more noise, but this is much more variable and unpredictable. In our application, receivers will usually be located in areas far from man-made noise sources and high thunderstorm areas. We therefore assume that the noise is due to atmospherics, which are due to distant thunderstorm activity.

The short-time noise model we use assumes the form

$$a(t) = A\, e^{n(t)} \cos\left[2\pi f_o t + \theta(t)\right] \quad , \tag{49}$$

where $n(t)$ is a stationary Gaussian process, $\theta(t)$ is a stationary random process independent of $n(t)$, and A is a constant. As we have shown in Part One, this noise model agrees well with available data, including second-order level-crossing data. The agreement is particularly good for large fluctuations of amplitude. Since large fluctuations of noise amplitude are more important than average noise in terms of causing errors in any system, it is particularly important to model this region accurately. We note that for small fluctuations the experimental data show the noise to behave like a Gaussian process. Although our model does not give Gaussian noise at small fluctuations, we make use of the above experimental result as a justification for one of our assumptions.

Consider next some of the properties of this noise model and their relation to measured noise parameters. The phase random variable at time t is uniformly distributed over $[0, 2\pi]$. Hence at any time we have

$$\begin{aligned} \overline{a^2(t)} &= A^2\, \overline{e^{2n(t)}}\ \overline{\cos^2\left[2\pi f_o t + \theta(t)\right]} \\ &= A^2\, \tfrac{1}{2}\, e^{2\sigma_n^2} \end{aligned} \quad , \tag{50}$$

where

$$\overline{\cos^2\left[2\pi f_o t + \theta(t)\right]} = \frac{1}{2} \tag{51}$$

$$\sigma_n^2 = \overline{n^2(t)} \quad . \tag{52}$$

Although we have assumed stationarity in our short-time noise model, it is clear that there are diurnal and seasonal variations in the noise characteristics. These slow variations can be accounted for in the two basic parameters of our short-time noise model given by A and σ_n^2.

To relate A and σ_n^2 to important measured noise parameters, we now note that the noise model is valid for the atmospheric noise that has been filtered through a receiver front-end filter of bandwidth W. In our application, W is between 200 Hz and 1000 Hz. Assuming that the atmospheric noise before filtering is approximately flat in spectrum over the filter bandwidth, we have

$$\overline{a^2(t)} = \frac{1}{2} A^2 e^{2\sigma_n^2} = N_o W \tag{53}$$

where N_o is the noise spectral density per unit bandwidth. The envelope of the process is

$$E(t) = A\, e^{n(t)} \tag{54}$$

which has an average value

$$\overline{E(t)} = A\, e^{\frac{1}{2}\sigma_n^2} \tag{55}$$

and an rms value

$$\sqrt{\overline{E^2(t)}} = A\, e^{\sigma_n^2} \quad . \tag{56}$$

A measure of the variability of the noise fluctuations is the quantity V_d, defined as

$$V_d = 20 \log_{10} \frac{\sqrt{E^2(t)}}{E(t)}$$
$$= 20\left(\frac{\sigma_n^2}{2}\right)\log_{10} e \qquad (57)$$
$$= 10\ \sigma_n^2 \log_{10} e \quad .$$

Equations (53) and (57) relate the parameters of our noise model (A, σ_n) to the well-known atmospheric noise parameters, V_d and F_a (effective antenna noise figure which is simply related to N_o).

A quantity of interest later is the probability that at any given time t the envelope E(t) will exceed some level B > 0. In particular, consider the event

$$H(B) = \left\{E(t) = A\ e^{n(t)} > B\right\} \qquad (58)$$

and the probability of this event

$$P_B = P_r\{H(B)\} \quad . \qquad (59)$$

The event H(B) is equivalent to the event

$$\left\{n(t) > \log_e \frac{B}{A}\right\} \quad , \qquad (60)$$

so

$$P_B = P_r\left\{n(t) > \log_e \frac{B}{A}\right\}$$
$$= \Phi\left(\frac{\log_e \frac{B}{A}}{\sqrt{\sigma_n^2}}\right) \quad , \qquad (61)$$

where

$$\Phi(x) = \int_x^\infty \frac{1}{\sqrt{2\pi}} \exp\left\{-\frac{t^2}{2}\right\} dt = 1 - \Psi(x) \quad . \qquad (62)$$

If the envelope E(t) is restricted to be less than or equal to B, then the resultant envelope c(t) is

$$c(t) = \begin{cases} A\ e^{n(t)} & \text{if not } H(B) \\ B & \text{if } H(B) \end{cases} \tag{63}$$

with probability density

$$p_c(x) = \delta(x - B)P_B + \left[1 - u_B(x)\right] p_n\left[\log_e(x/A)\right] \tag{64}$$

where

$$p_n(x) = \frac{1}{\sqrt{2\pi\sigma_n^2}} \exp\left\{-\frac{x^2}{2\sigma_n^2}\right\} , \tag{65}$$

$$u_B(x) = \begin{cases} 1 & x > B \\ 0 & x < B \end{cases} , \tag{66}$$

and $\delta(x)$ is the Dirac delta function. The mean square of this "clipped" envelope is

$$\begin{aligned} \overline{c^2} &= \int_{-\infty}^{\log_e(B/A)} \frac{A^2}{\sqrt{2\pi\sigma_n^2}} \exp\left\{2\alpha - \frac{\alpha^2}{2\sigma_n^2}\right\} d\alpha + B^2 P_B \\ &= A^2\, e^{2\sigma_n^2} \int_{-\infty}^{\log_e(B/A)} \frac{1}{\sqrt{2\pi\sigma_n^2}} \exp\left\{-\frac{\left(\alpha - 2\sigma_n^2\right)^2}{2\sigma_n^2}\right\} d\alpha + B^2 P_B \\ &= A^2\, e^{2\sigma_n^2} \left\{1 - \Phi\left(\frac{\log_e(B/A) - 2\sigma_n^2}{\sqrt{\sigma_n^2}}\right)\right\} + B^2 P_B \end{aligned} \tag{67}$$

Using Eq. (61) for P_B we have

$$\overline{c^2} = A^2 e^{2\sigma_n^2} \left\{ 1 - \Phi\left(\frac{\log_e(B/A) - 2\sigma_n^2}{\sqrt{\sigma_n^2}} \right) \right\} + B^2 \Phi\left(\frac{\log_e(B/A)}{\sqrt{\sigma_n^2}} \right) \quad . \quad (68)$$

This noise model is used to compute the desired error probabilities. The parameters A and σ_n^2 are obtained from measured and predicted values of F_a and V_d. Equation (68) is used to approximate the effects of clipping on the received noise.

III SIGNAL REPRESENTATION

The modulation system to be used at VLF is strongly limited by the characteristics of the high-power amplifiers and high-efficiency antennas that constitute present stationary VLF transmitters. The most desirable modulation signals would maximize the information transmitted in the allowed bandwidth through a noisy channel for given fixed peak power. Given a peak power limitation, the highest average power is radiated when the transmitted wave has a constant envelope. An additional factor that necessitates a constant envelope is the final RF amplifier. Existing high-power VLF facilities use Class C amplifiers because of their efficiency; this mode of operation requires constant envelope and continuous phase for highest efficiency. Discontinuity in envelope or phase of an RF wave also causes large transients in the transmitter output. Transient response of the transmitting system depends upon the system bandwidth, which at VLF is generally limited by the high Q inherent to the most efficient transmitting antennas.

Because of practical limitations on the transmitters at VLF and LF, we consider only angle-modulated signals, with emphasis on those that are phase continuous. In particular, we restrict our attention to binary FSK, PSK, and MSK signaling schemes. One exception that we consider is on-off CW keying.

During a signaling time of T seconds, one of two signals will be transmitted. Letting H_o be the hypothesis that a signal corresponding to "zero" is transmitted and H_1 be the hypothesis that a "one" signal is sent, we have

$$H_o: \quad m_o(t) = \sqrt{2P}\cos\left[2\pi f_o t + \theta_o(t)\right] \tag{69}$$

$$H_1: \quad m_1(t) = \sqrt{2P}\cos\left[2\pi f_o t + \theta_1(t)\right] \tag{70}$$

as the two types of signal. For FSK we have

$$\theta_o(t) = \Delta\omega t$$

and (71)

$$\theta_1(t) = -\Delta\omega t \quad .$$

Note that the average power for both signals is P, and let ρ be the correlation between $m_o(t)$ and $m_1(t)$. Hence

$$\rho = \frac{1}{PT}\int_0^T m_o(t)m_1(t)\,dt \quad . \tag{72}$$

The signals we consider have the general form given by Eqs. (69) and (70). At the receiver the received signal has the form

$$\begin{aligned} H_o: &\quad r(t) = m_o(t) + a(t) \quad t\in[0,T] \\ H_1: &\quad r(t) = m_1(t) + a(t) \quad t\in[0,T] \quad . \end{aligned} \tag{73}$$

An exception to this simple binary signaling is on-off keying and the two AJ signaling schemes which consist of long sequences of such binary pulses.

IV COHERENT BINARY RECEIVER MODEL

We now consider how the coherent receiver processes the signal $r(t)$, $t\epsilon[0,T]$ to determine which binary signal was sent. If the noise $a(t)$, $t\epsilon[0,T]$ is a Gaussian process, then the minimum-probability-of-error receiver has the form shown in Fig. 10. Recall that $a(t)$, $t\epsilon[0,T]$ is in our case a non-Gaussian process which is impulsive in character.

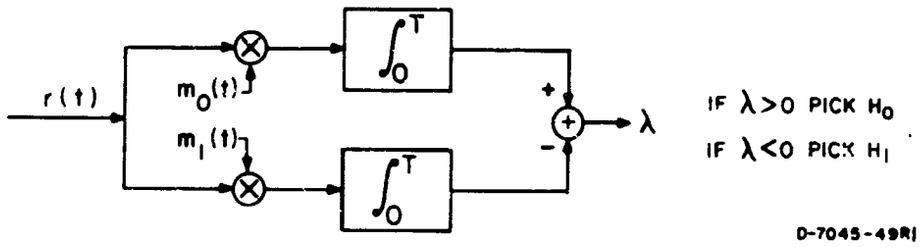

FIGURE 10 COHERENT RECEIVER MODEL—NO CLIPPING

Since the noise fluctuation often exceeds the signal peak, in many receivers a nonlinear clipping function is introduced in the receiving system before the correlation stage. Thus receivers typically have the form given by Fig. 11, where

$$r'(t) = \begin{cases} B & y(t) > B \\ y(t) & -B \le y(t) \le B \\ -B & y(t) < -B \end{cases} \quad . \tag{74}$$

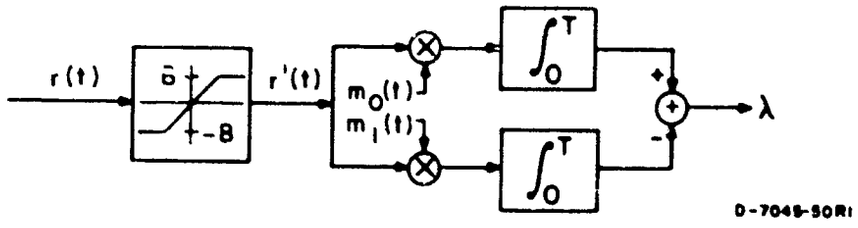

FIGURE 11 COHERENT RECEIVER MODEL—CLIPPING

On the basis of our assumed noise model, the optimum maximum likelihood receiver will certainly be different from the above receiver. Indeed, the above receiver is not an optimum receiver for any known noise model; rather, it evolved from classical Gaussian noise receivers with the nonlinearity introduced to get rid of the non-Gaussian impulsiveness of the noise.

The nonlinear clipping of the received signal is difficult to analyze. Watt,[25] however, has shown that if the clipping level is greater than the signal peak then most of the slipping effect is on the noise peaks. He has shown experimentally that the distribution of signal and atmospheric noise at a level twice or more above the signal peak is approximately the result of noise only. We therefore make the assumption that when the clipping level is above the signal peak only the noise signal peaks are clipped. When one considers the impulsive nature of the noise and the fact that the nonlinear clipper is designed to clip high noise peaks, this assumption is reasonable. The resulting signal is shown in Fig. 11, where

$$\begin{aligned} r(t) &= A\, e^{n(t)} \cos\left[2\pi f_o t + \theta(t)\right] + m(t) \\ r'(t) &= c(t) \cos\left[2\pi f_o t + \vartheta(t)\right] + m(t) \end{aligned} \qquad (75)$$

where $m(t)$ is either $m_o(t)$ or $m_1(t)$, and $c(t)$ is given by Eq. (63).

After passing through the nonlinear clipper, the received clipped signal is now processed in the usual correlator receiver, which computes a likelihood function λ on which it bases a decision. Since correlation is a linear operation, if the noise process

$$c(t) \cos\left[2\pi f_o t + \vartheta(t)\right] \qquad (76)$$

is Gaussian, then λ is a Gaussian random variable. Even if the noise process is non-Gaussian, if the integration time T is large compared to the correlation time of the noise process, λ approaches a Gaussian

random variable in distribution. This approximation gets better as T increases. The correlation time of the noise process is roughly

$$\tau = \frac{1}{2W} \quad , \tag{77}$$

which for W = 1000 Hz is 0.5 ms. We consider the signal time for each bit of approximately 20 ms to be roughly 40 correlation times. Recall that for small fluctuations the atmospheric noise process has a Gaussian distribution (Rayleigh envelope) and that large fluctuations which could normally change the distribution of the likelihood ratio λ have been clipped so that their effect on λ is reduced. These arguments lead us to conclude that, although the clipped noise process given by Expression (76) is Gaussian only for small fluctuations, because of clipping and the large integration time, λ can be approximated as a Gaussian random variable. Certainly this approximation is less accurate for the tails of the distribution of λ. Determination of the accuracy of this assumption is beyond the scope of this study. We also see that, because of uncertainties in determining signal and noise parameters, more accuracy in the error expression is not worth the additional effort.

From Fig. 11 we see that λ is given by

$$\lambda = \int_0^T r'(t)\left[m_o(t) - m_1(t)\right] dt \quad , \tag{78}$$

where

$$r'(t) = c(t) \cos\left[2\pi f_o t + \theta(t)\right] + m(t) \quad . \tag{79}$$

Suppose that H_1 is true and consequently that $m(t) = m_1(t)$. Then we have

$$\lambda = \int_0^T c(t) \cos\left[2\pi f_o t + \theta(t)\right]\left|m_o(t) - m_1(t)\right| dt + (\rho - 1)\, PT \quad . \tag{80}$$

An error or wrong decision occurs if λ is greater than zero. This event occurs with probability P_e, given by

$$P_e = P_r\{\lambda > 0 | H_1\} \quad . \tag{81}$$

Defining

$$a'(t) = c(t) \cos\left[2\pi f_o t + \theta(t)\right] \tag{82}$$

and

$$g = \int_0^T a'(t)\{m_o(t) - m_1(t)\}\, dt \quad , \tag{83}$$

we have

$$P_e = P_r\{g > (1 - \rho)\, PT | H_1\} \quad . \tag{84}$$

Clearly,

$$\bar{g} = 0 \tag{85}$$

and

$$\sigma_g^2 = \overline{g^2} = \int_0^T \int_0^T \overline{a'(\alpha)a'(\beta)}\{m_o(\alpha) - m_1(\alpha)\}\{m_o(\beta) - m_1(\beta)\}\, d\alpha d\beta \quad . \tag{86}$$

The noise process $a'(t)$ is essentially white compared to the narrow-band signals $m_o(t)$ and $m_1(t)$. Hence

$$\overline{a'(\alpha)a'(\beta)} = \frac{\overline{a'^2(\alpha)}}{2W}(2W)\frac{\sin 2\pi W(\alpha - \beta)}{2\pi W(\alpha - \beta)} \tag{87}$$

is like a Dirac delta function in Eq. (86). This gives

$$\sigma_g^2 = \frac{\overline{a'^2(\alpha)}}{2W}\int_0^T \left[m_o(\alpha) - m_1(\alpha)\right]^2 d\alpha$$

$$\sigma_g^2 = \frac{\overline{a'^2(\alpha)}}{2W} 2(1 - \rho)\, PT \quad . \tag{88}$$

We know that

$$\lim_{W\to\infty} 2W \frac{\sin 2\pi Wt}{2\pi Wt} = \delta(t) \quad . \tag{89}$$

For the front-end bandwidth W sufficiently large that $m_o(t)$ and $m_1(t)$ remain unchanged by the front-end filter, this assumption is valid. But

$$\overline{a'^2(\gamma)} = \overline{c^2(t)}\ \overline{\cos^2\left[2\pi f_o t + \vartheta(t)\right]} \tag{90}$$

$$= \frac{1}{2}\overline{c^2(t)}$$

Hence

$$\sigma_g^2 = \frac{1}{2W}\overline{c^2(t)}\ (1 - \rho)\ PT \quad . \tag{91}$$

The error probability is then

$$P_e = P_r\left\{\frac{n}{\sqrt{\sigma_g^2}} > \sqrt{\frac{2PT(1-\rho)}{\overline{c^2}/W}}\right\} \tag{92}$$

$$= \tfrac{1}{2}\left(\sqrt{\frac{2PWT(1-\rho)}{\overline{c^2}}}\right) \quad .$$

By symmetry we see that the error probability when m_o is sent is the same. Hence P_e represents the total error probability. By collecting all terms this is given by

$$P_e = \tfrac{1}{2}\left(\sqrt{\frac{2PWT(1-\rho)}{\overline{c^2}}}\right) \quad , \tag{93}$$

where

$$\overline{c^2} = A^2 e^{-2\frac{\sigma_n^2}{B}}\left\{1 - \tfrac{1}{2}\left(\frac{\log_e(B/A) - 2\frac{\sigma_n^2}{B}}{\sqrt{\sigma_n^2}}\right)\right\} \tag{94}$$

$$+ B^2\ \tfrac{1}{2}\left(\frac{\log_e(B/A)}{\sqrt{\sigma_n^2}}\right) \quad ,$$

$$N_o W = \frac{1}{2} A^2 e^{2\sigma_n^2} \quad , \tag{95}$$

and

$$V_d = 10\ \sigma_n^2 \log_{10} e \quad . \tag{96}$$

Although not all the receivers we consider have a nonlinear clipper in the front, nonintentional clipping often occurs when the dynamic range of the receiver is exceeded by a noise spike. Consequently, Eq. (94) should still be valid without a clipper if the clip level B is chosen to be as large as the maximum signal level. Note that

$$\lim_{B\to\infty} \Phi\left(\frac{\log_e(B/A) - 2\sigma_n^2}{\sqrt{\sigma_n^2}}\right) = 0 \tag{97}$$

and

$$\lim_{B\to\infty} B^2\ \Phi\left(\frac{\log_e(B/A)}{\sqrt{\sigma_n^2}}\right) = 0 \quad , \tag{98}$$

hence for large B, $\overline{c^2}$ approaches

$$\lim_{B\to\infty} \overline{c^2} = A^2 e^{2\sigma_n^2} \quad , \tag{99}$$

being the same as the case for no clipping.

The probability-of-error expression of Eq. (93) applies for coherent FSK, PSK, and MSK signaling schemes. We have developed this expression here mainly to present a representative calculation of probability of error and to point out the assumptions made throughout the remainder of Part Two. Although the error calculations may differ for other communication systems of interest, many of the results of this chapter are referred to in later chapters. We now consider specific modulation-demodulation schemes, then compute error probabilities, and finally plot curves of these probabilities for typical parameters.

V PROBABILITY-OF-ERROR CALCULATIONS

This chapter develops probability-of-error expressions for various generic modulation-demodulation systems. These systems and the parameters chosen correspond roughly to existing and planned future VLF/LF communication systems.

In all cases, we consider modulation-demodulation systems for binary signals denoting Marks and Spaces. We denote T as the time duration of a single-channel binary signal. In some cases an information bit may require the transmission of several channel bits (sometimes referred to as "chips"). We also assume that the noise in the channel has a constant spectral density over the bandwidth, W, of the receiver's front-end bandpass filter. This spectral density is denoted as N_o watts per hertz. In all cases signal power is constant and given by P watts per second.

Throughout most of this chapter we assume that the signaling time is much greater than 1/W, so the test statistics upon which a decision is based can be approximated as Gaussian random variables. With clipping introduced, this assumption is even more accurate, since large noise peaks are eliminated, and low noise levels which pass through the clipper behave like Gaussian noise. This Gaussian assumption is especially good for an interesting case where integration times are very long compared to 1/W. In the Appendix we take the case where $T < 1/W$ and W is greater than a few hundred hertz. Hall[15] calls this case the "short-duration" signal and notes that it is very uncommon at VLF and LF. In this case we use the approach of Bello[26] to compute error probabilities.

A. Binary On-Off Keying (CW)

On-off keying is perhaps the simplest modulation technique for transmitting binary information. An on-off-keyed radio system can be described as transmitting pulses

$$m(t) = \begin{cases} \sqrt{2P}\,\sin(\omega_o t + \Phi) & \text{for Mark} \\ 0 & \text{for Space} \end{cases} \qquad (100)$$

where the signal duration is T seconds, and the power of the Mark pulse is P.

The signal (Mark or Space) is transmitted over a channel which adds atmospheric noise of constant spectral density N_o over the receiver front-end bandwidth, W. We consider two types of noncoherent receiver systems, one with clipping in the front end and one without clipping.

We first consider a noncoherent receiver with no clipping. This consists of a bandpass filter matched to the Mark pulse (except for an unknown phase), followed by an envelope detector sampled at time T as shown in Fig. 12, where

$$h(t) = \sqrt{\frac{2}{T}}\,\sin\,\omega_o(T - t) \qquad t \in [0,T] \quad .$$

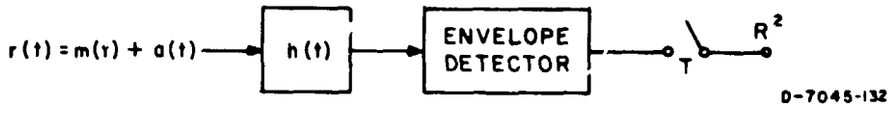

FIGURE 12 NONCOHERENT DETECTION OF CW PULSE—NO CLIPPING

The sampled test statistic, R^2, is given by

$$R^2 = r_s^2 + r_c^2 \quad , \qquad (101)$$

where

$$r_s = \sqrt{\frac{2}{T}} \int_0^T r(t)\,\sin\,\omega_o t\,dt$$

$$r_c = \sqrt{\frac{2}{T}} \int_0^T r(t)\,\cos\,\omega_o t\,dt \qquad (102)$$

The decision rule is to compare R^2 with a threshold as follows:

$$\begin{aligned} R^2 &> \delta^2 \quad \text{choose Mark} \\ R^2 &\leq \delta^2 \quad \text{choose Space} \end{aligned} \tag{103}$$

If a Mark is sent, we have

$$r(t) = \sqrt{2P}\,\sin\left[\omega_o t + \theta\right] + a(t) \tag{104}$$

and

$$\begin{aligned} r_s &= \sqrt{PT}\,\sin\theta + n_s \\ r_c &= \sqrt{PT}\,\cos\theta + n_c \end{aligned} \tag{105}$$

where

$$n_s = \int_0^T a(t)\,\sqrt{\frac{2}{T}}\,\sin\omega_o t\,dt \tag{106}$$

and

$$n_c = \int_0^T a(t)\,\sqrt{\frac{2}{T}}\,\cos\omega_o t\,dt \tag{107}$$

are approximated as independent Gaussian random variables with zero mean and variance $N_o/2$. This assumes that T is large enough to include many independent samples of the noise. Under this assumption the random variable R^2 is a noncentral chi-square random variable of order 2. When Mark is sent, the error probability is

$$\begin{aligned} P_{e_1} &= P_r\left[R^2 = r_s^2 + r_c^2 \leq \delta^2 \,\middle|\, \text{Mark}\right] \\ &= 1 - Q\left(\sqrt{\frac{2PT}{N_o}}\,,\ \sqrt{\frac{2\delta^2}{N_o}}\right) \end{aligned} \tag{108}$$

where

$$Q(a,b) = \int_b^\infty t \exp\left\{-\frac{t^2 + a^2}{2}\right\} I_o(at)\, dt \tag{109}$$

is the Marcum Q-function.[27] If a Space is sent, we have

$$\begin{aligned} r_s &= n_s \\ r_c &= n_c \quad , \end{aligned} \tag{110}$$

and R^2 is a chi-square random variable of order 2. When Space is sent, the error probability is given by

$$\begin{aligned} P_{e_o} &= P_r\left\{R^2 = r_s^2 + r_c^2 > \delta \,|\, \text{Space}\right\} \\ &= \exp\left\{-\frac{\delta^2}{N_o}\right\} \quad . \end{aligned} \tag{111}$$

Assuming that Marks and Spaces occur with equal probability, the total unconditioned binary error probability is

$$P_e = \frac{1}{2} - \frac{1}{2} Q\left(\sqrt{\frac{2PT}{N_o}} \;,\; \sqrt{\frac{2\delta^2}{N_o}}\right) + \frac{1}{2} \exp\left\{-\frac{\delta^2}{2}\right\} \quad . \tag{112}$$

Figure 13 gives this error versus signal-to-noise ratio, PT/N_o, for various normalized thresholds, $b = \sqrt{2\delta^2/N_o}$.

Stein and Jones[28] show that the threshold δ^2 that minimizes the error probability is approximately

$$\delta^2 = N_o + \frac{PT}{4} \quad , \tag{113}$$

which gives a minimum error probability

$$P_e = \frac{1}{2} - \frac{1}{2} Q\left(\sqrt{\frac{2PT}{N_o}} \;,\; \sqrt{2 + \frac{PT}{2N_o}}\right) + \frac{1}{2} \exp\left\{-\left(1 + \frac{PT}{4N_o}\right)\right\} \quad . \tag{114}$$

This is also plotted in Fig. 13.

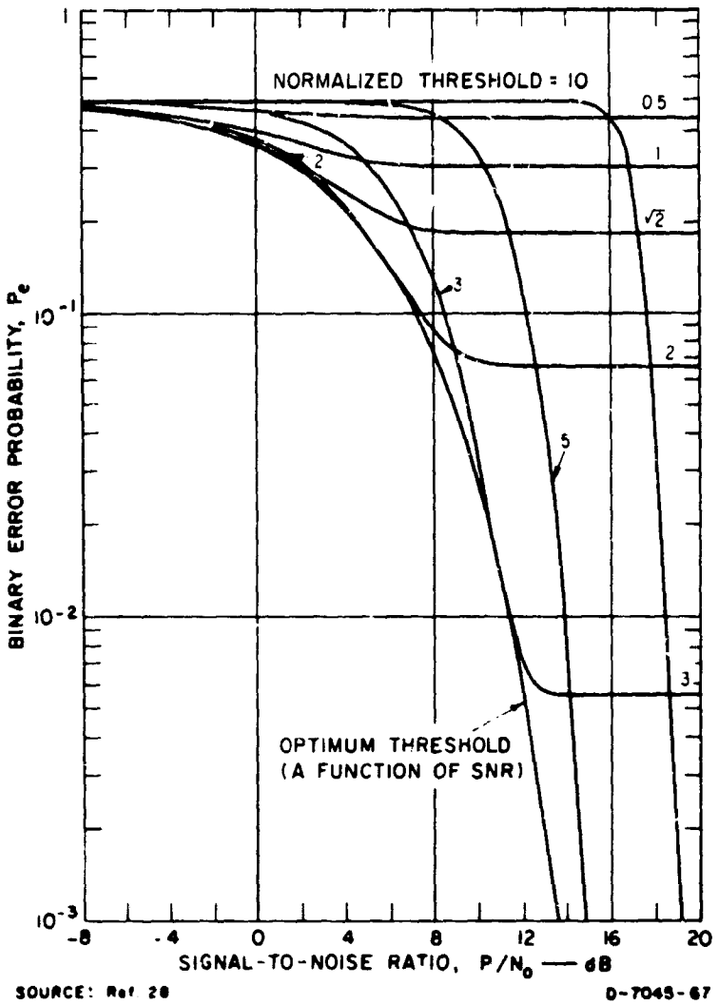

FIGURE 13 BINARY ERROR PROBABILITY FOR ON-OFF KEYING—NO CLIPPING

For large signal-to-noise ratio

$$\frac{PT}{4N_0} \gg 1 \quad , \tag{115}$$

we have

$$Q\left(\sqrt{\frac{2PT}{N_0}} \cdot \sqrt{2 + \frac{PT}{2N_0}}\right) \approx 1 - \Phi\left(\sqrt{\frac{PT}{2N_0}}\right) \quad . \tag{116}$$

where

$$\Phi(a) = \int_a^\infty \frac{1}{\sqrt{2\pi}} \exp\left\{-\frac{t^2}{2}\right\} dt \qquad (117)$$

is well-tabulated.[21] For large signal-to-noise ratio, we thus have

$$P_e \cong \frac{1}{2}\,\Phi\left(\sqrt{\frac{PT}{2N_o}}\right) + \frac{1}{2}\exp\left\{-\frac{PT}{4N_o}\right\} \quad . \qquad (118)$$

For the receiver with front-end clipping, we have the situation shown in Fig. 14. This receiver differs from the previous case in that

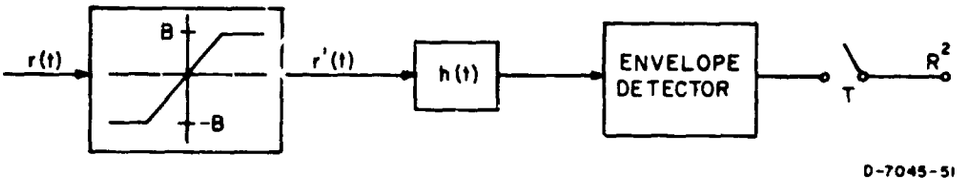

FIGURE 14 NONCOHERENT DETECTION OF CW PULSE—CLIPPING

r(t) is clipped for $|r(t)| \geq B$. As shown in the previous chapter, when

$$B \sim 2\sqrt{2P} \quad , \qquad (119)$$

most of the portion of the signal that is clipped is the part of the received signal that is due to high noise peaks. We therefore assume that the clipper output is approximated by

$$r'(t) = m(t) + a'(t) \quad , \qquad (120)$$

where

$$a'(t) = c(t)\sin\left[\omega_o t + \vartheta(t)\right] \quad , \qquad (121)$$

as in Eq. (79). The clipped noise is assumed to have spectral density

$$N_o' = \frac{\overline{c^2}}{2W} \quad , \tag{122}$$

where $\overline{c^2}$ is given by Eq. (94).

Using the new noise density N_o' after clipping, we have the error expression

$$P_e = \frac{1}{2} - \frac{1}{2} Q\left(\sqrt{\frac{2PT}{N_o'}} \ , \ \sqrt{\frac{2\delta^2}{N_o'}}\right) + \frac{1}{2} \exp\left\{-\frac{\delta^2}{N_o'}\right\} \quad . \tag{123}$$

This expression depends on signal-to-noise ratio, P/N_o, detection threshold, δ^2, clipping level, β, receiver front bandwidth, W, signal duration, T, and noise parameter, V_d. In Fig. 15 we plot P_e versus P/N_o for optimum thresholds and T = 0.02, W = 1000 Hz, β = 2, β = 4, and various values of V_d.

L. Binary Frequency-Shift Keying (FSK)

One of the most common type of binary signaling schemes is the FSK signaling scheme with a modulation index of one. This scheme results in a Mark-Space signal sequence which has constant amplitude and continuous phase. The two signal pulses are

$$\begin{aligned} m_1(t) &= \sqrt{2P} \sin\left[\omega_o t + \Delta\omega t\right] \quad \text{for Mark} \\ m_o(t) &= \sqrt{2P} \sin\left[\omega_o t - \Delta\omega t\right] \quad \text{for Space} \quad , \end{aligned} \tag{124}$$

where

ω_o is the center frequency and

$\Delta\omega = \pi/T$, both in radians per second.

This frequency deviation, $\Delta\omega$, corresponds to a modulation index of one and results in the two pulses $m_1(t)$ and $m_o(t)$ being orthogonal. That is,

$$\int_0^T m_o(t) m_1(t)\, dt = 0 \quad . \tag{125}$$

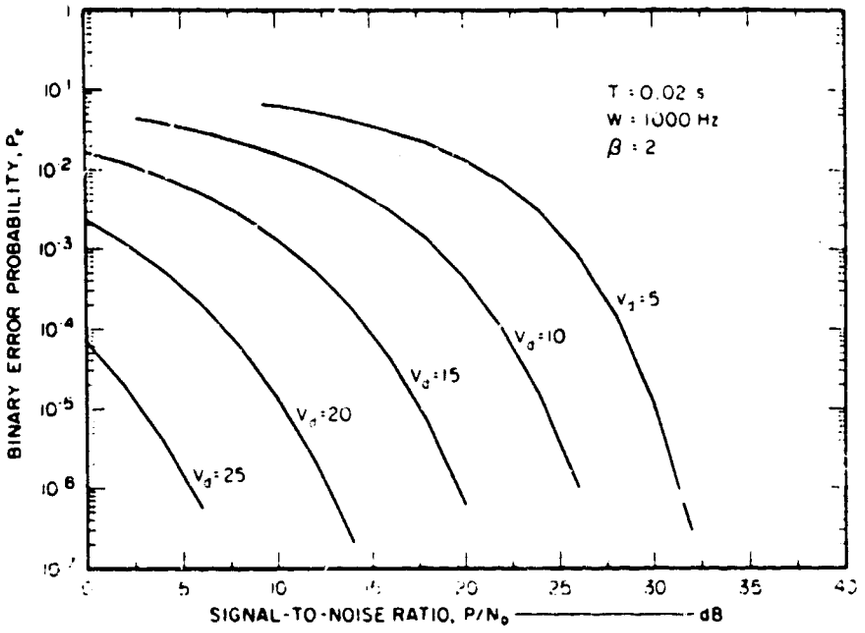

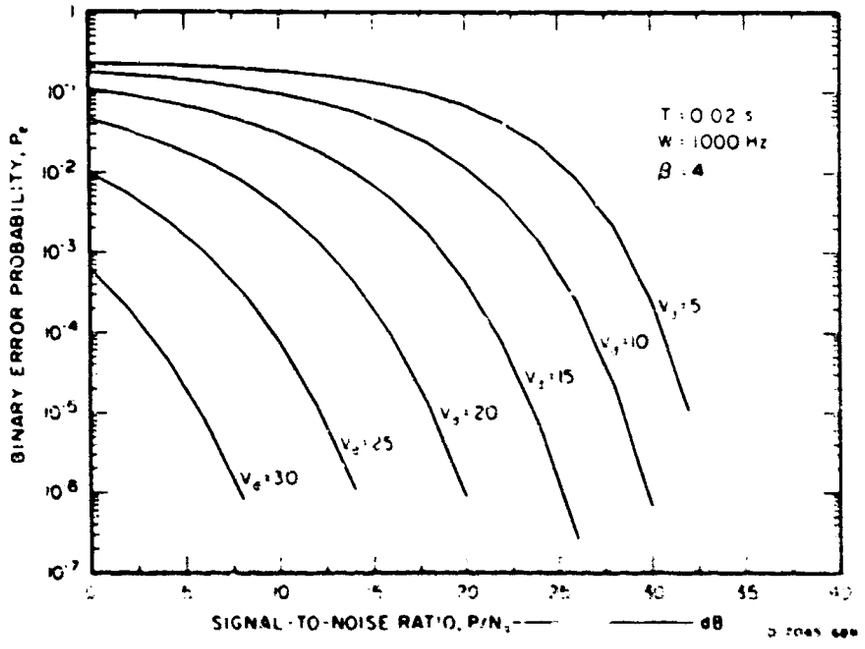

FIGURE 15 BINARY ERROR PROBABILITY FOR ON-OFF KEYING—CLIPPING

We consider coherent and noncoherent detection of these FSK signals under the two conditions of clipping and no clipping in the front end of the receiving system. Classical coherent detection without any nonlinear clipping is diagrammed in Fig. 16, where

$$h_1(t) = \sqrt{\frac{1}{PT}}\, m_1(T - t)$$
$$h_o(t) = \sqrt{\frac{1}{PT}}\, m_o(T - t) \quad . \tag{126}$$

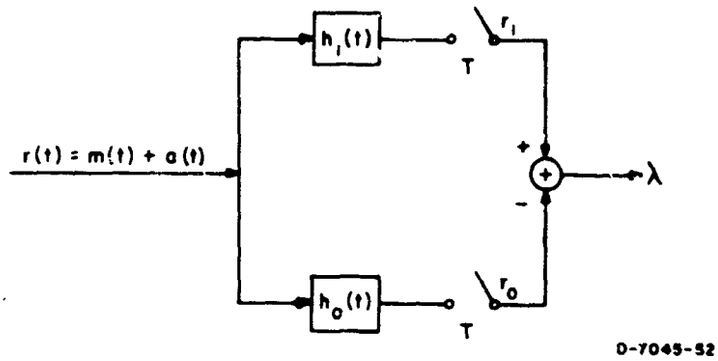

FIGURE 16 COHERENT DETECTION OF FSK—NO CLIPPING

The sampled test statistic is given by

$$\lambda = r_1 - r_o \quad ,$$

where

$$r_1 = \int_0^T r(t) \sqrt{\frac{2}{T}} \sin\left[\omega_o t + \omega_1 t\right] dt$$
$$r_o = \int_0^T r(t) \sqrt{\frac{2}{T}} \sin\left[\omega_o t - \omega_1 t\right] dt \quad . \tag{127}$$

The decision rule is to compare λ with zero, as follows,

$$\begin{aligned} \lambda > 0 \quad & \text{choose Mark} \\ \lambda \leq 0 \quad & \text{choose Space} \quad , \end{aligned} \tag{128}$$

where, as usual, we assume that Marks and Spaces occur with equal probability. Note that the coherent receiver is merely another representation of the correlation receiver of Fig. 10. The error probability with no clipping is given by Eq. (93) with $\rho = 0$ and $\overline{c^2} = A^2 e^{2\sigma_n^2}$. Hence

$$P_e = \Phi\left(-\sqrt{\frac{PT}{N_o}}\right) \quad , \tag{129}$$

since

$$A^2 e^{2\sigma_n^2} = 2N_o W \quad . \tag{130}$$

With clipping in the front end we have, from Eq. (93) with $\rho = 0$,

$$P_e = \Phi\left(-\sqrt{\frac{2PWT}{\overline{c^2}}}\right) \quad , \tag{131}$$

where

$$\overline{c^2} = A^2 e^{2\sigma_n^2}\left\{1 - \Phi\left(\frac{\log_e(B/A) - 2\sigma_n^2}{\sqrt{\sigma_n^2}}\right)\right\} + B^2 \Phi\left(\frac{\log_e(B/A)}{\sqrt{\sigma_n^2}}\right) \tag{132}$$

$$\begin{aligned} N_o W &= \frac{1}{2} A^2 e^{2\sigma_n^2} \\ V_d &= 10\, \sigma_n^2 \log_{10} e \quad . \end{aligned} \tag{133}$$

Choosing

$$B = \beta\sqrt{2P} \quad , \tag{134}$$

we rewrite P_e in terms of parameters P, N_o, β, V_d, T, and W:

$$P_e = \Phi\left(\left[\frac{PT}{N_o\left[1 - \Phi(D) + \beta^2 \frac{P}{N_o W} \Phi(E)\right]}\right]^{\frac{1}{2}}\right) , \tag{135}$$

where

$$D = \frac{20 \log_e(\beta/\sqrt{W}) + 10 \log_e(P/N_o) - 2V_d \log_e 10}{20\sqrt{\frac{V_d}{10} \log_e 10}} \tag{136}$$

and

$$E = \frac{20 \log_e(\beta/\sqrt{W}) + 10 \log_e(P/N_o) + 2V_d \log_e 10}{20\sqrt{\frac{V_d}{10} \log_e 10}} . \tag{137}$$

Figure 17 plots P_e for FSK signals for various parameters of interest. Here β represents the clipping level above the signal peak of $\sqrt{2P}$. For example, $\beta = 2$ means that the clipping level is set at $B = 2\sqrt{2P}$ or twice the signal peak amplitude.

For noncoherent detection without clipping, we have filters matched to the Mark and Space pulses (except for an unknown phase), followed by envelope detectors sampled at time T, as shown in Fig. 18, where the sampled test statistic Δ is given by

$$\begin{aligned} \Delta &= R_1^2 - R_o^2 \\ R_1^2 &= r_{1s}^2 + r_{1c}^2 \\ R_o^2 &= r_{os}^2 + r_{oc}^2 \end{aligned} \tag{138}$$

The terms r_{1s} and r_{1c} are the sine and cosine components of the received signal relative to the Mark frequency. Similarly, r_{os} and r_{oc} are the components relative to the Space frequency.

Recalling that $m_1(t)$ and $m_o(t)$ are orthogonal or uncorrelated, we see that the matched filters $h_1(t)$ and $h_o(t)$ are also orthogonal. This

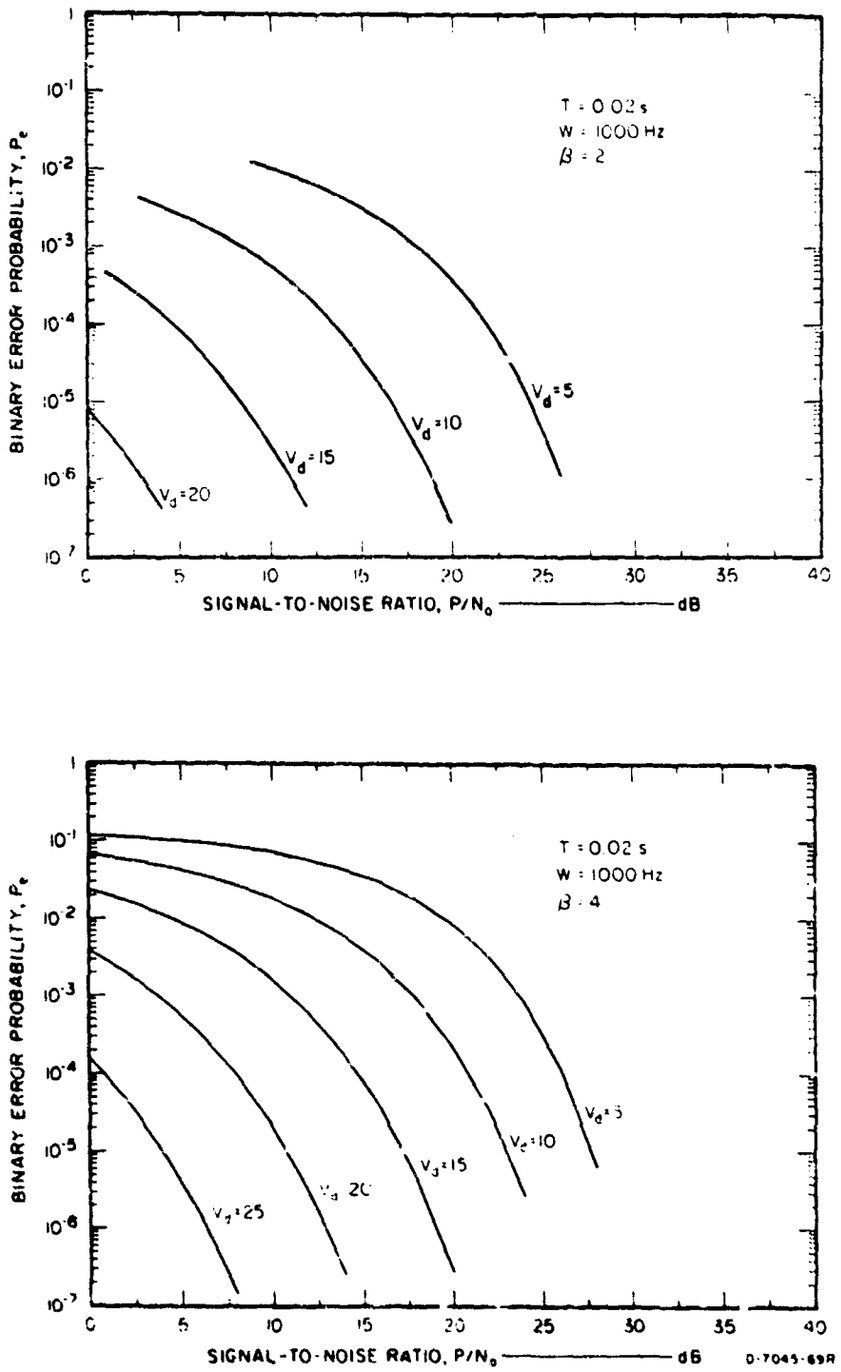

FIGURE 17 BINARY ERROR PROBABILITY FOR COHERENT FSK—CLIPPING

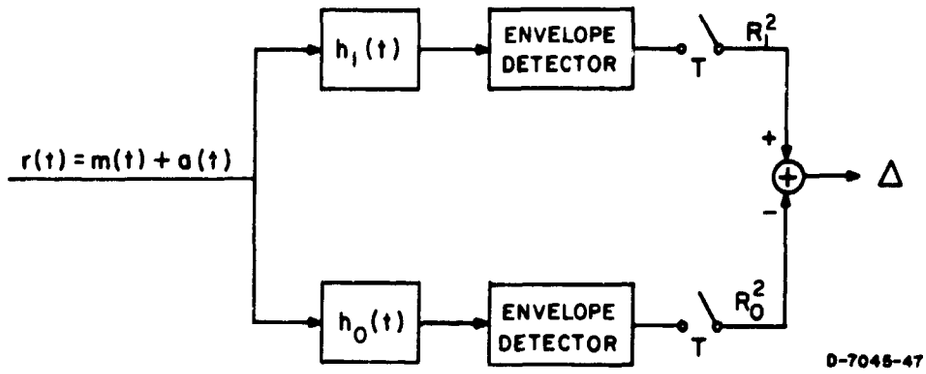

FIGURE 18 NONCOHERENT DETECTION OF FSK—NO CLIPPING

means that the outputs at time T of the matched filters have noise components that are uncorrelated and, since they are assumed to be Gaussian random variables, independent. Assuming a Mark is sent, we then have R_1^2, a noncentral chi-square random variable, and R_0^2, a central chi-square random variable. Perhaps a conceptually simpler representation of the noncoherent receiver process is that given in Fig. 19, where

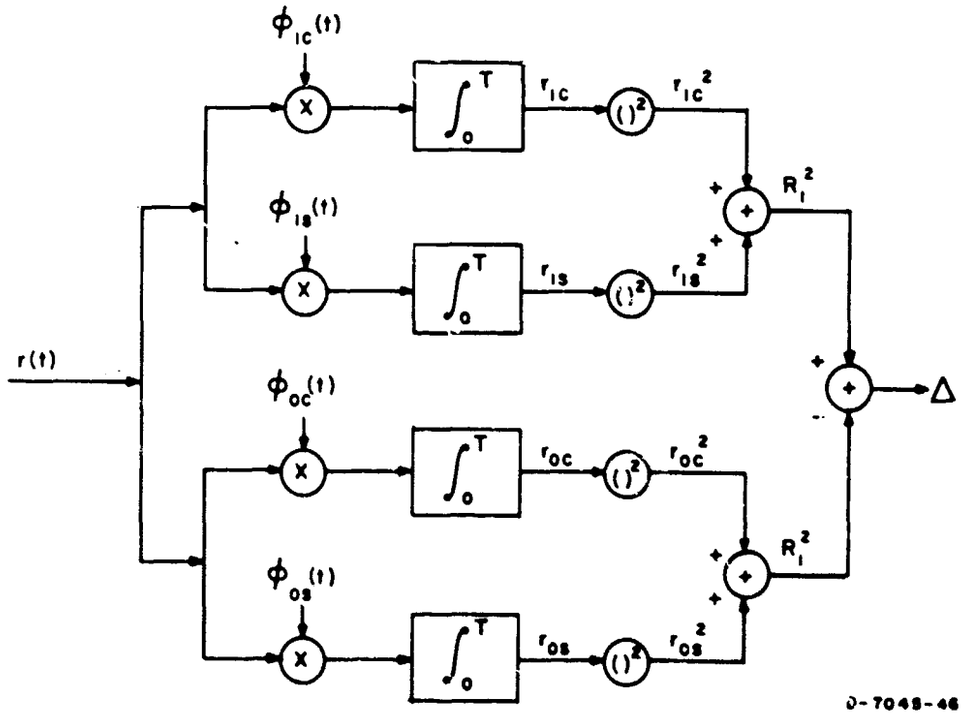

FIGURE 19 NONCOHERENT FSK DETECTOR REPRESENTATION

$$\begin{aligned}
\phi_{1c}(t) &= \sqrt{\frac{2}{T}} \cos\left[\omega_o t + \Delta\omega t\right] \\
\phi_{1s}(t) &= \sqrt{\frac{2}{T}} \sin\left[\omega_o t + \Delta\omega t\right] \\
\phi_{oc}(t) &= \sqrt{\frac{2}{T}} \cos\left[\omega_o t - \Delta\omega t\right] \\
\phi_{os}(t) &= \sqrt{\frac{2}{T}} \sin\left[\omega_o t - \Delta\omega t\right] \quad .
\end{aligned} \tag{139}$$

If a Mark is sent, the probability of error is found from the distribution of $R_1^2 - R_o^2$. First, define vectors

$$\underline{r}_1 = \begin{bmatrix} r_{1c} \\ \\ r_{1s} \end{bmatrix} \quad , \quad \underline{r}_o = \begin{bmatrix} r_{oc} \\ \\ r_{os} \end{bmatrix} \quad . \tag{140}$$

Since a Mark is sent, $\underline{r}_1$ consists of signal plus noise, while $\underline{r}_o$ consists of noise alone. Hence,

$$\underline{r}_1 = \begin{bmatrix} r_{1c} \\ \\ r_{1s} \end{bmatrix} = \begin{bmatrix} \sqrt{PT}\cos\theta + n_{1c} \\ \\ -\sqrt{PT}\sin\theta + n_{1s} \end{bmatrix} \tag{141}$$

$$= \underline{m} + \underline{n}_1$$

$$\underline{r}_o = \begin{bmatrix} r_{oc} \\ \\ r_{os} \end{bmatrix} = \begin{bmatrix} n_{oc} \\ \\ n_{os} \end{bmatrix} = \underline{n}_o \quad , \tag{142}$$

where θ is an unknown phase term, and n_{1c}, n_{1s}, n_{oc}, n_{os} are independent, zero-mean Gaussian random variables with common variance $N_o/2$. Using the notation

$$||\underline{r}_1||^2 = r_{1c}^2 + r_{1s}^2 \quad ,$$

we have

$$R_1^2 = ||\underline{r}_1||^2 = ||\underline{m} + \underline{n}_1||^2$$
$$R_o^2 = ||\underline{r}_o||^2 = ||\underline{n}_o||^2 \quad . \tag{143}$$

The probability of error is

$$\begin{aligned} P_e &= P_r\{\Delta < 0 | H_1\} \\ &= P_r\{R_1^2 - R_o^2 < 0 | H_1\} \\ &= P_r\{||\underline{m} + \underline{n}_1||^2 - ||\underline{n}_o||^2 < 0\} \\ &= P_r\{||\underline{m} + \underline{n}_1||^2 < ||\underline{n}_o||^2\} \\ &= \int_{-\infty}^{\infty}\int_{\infty}^{\infty} P_r\{||\underline{n}_o||^2 > ||\underline{m} + \underline{n}_1||^2 | \underline{n}_1 = \underline{\alpha}\} p_{\underline{n}_1}(\underline{\alpha})\, d\underline{\alpha} \quad . \end{aligned} \tag{144}$$

But

$$P_r\{||\underline{n}_o||^2 \geq R^2\} = \exp\left\{-\frac{R^2}{N_o}\right\} \quad , \tag{145}$$

so

$$P_r\{||\underline{n}_o||^2 \geq ||\underline{m} + \underline{n}_1||^2 | \underline{n}_1 = \underline{\alpha}\} = \exp\left\{-\frac{||\underline{m} + \underline{\alpha}||^2}{N_o}\right\} \quad . \tag{146}$$

Also,

$$p_{\underline{n}_1}(\underline{\alpha}) = \frac{1}{\pi N_o} \exp\left\{-\frac{||\underline{\alpha}||^2}{N_o}\right\} \quad . \tag{147}$$

Hence

$$P_e = \int_{-\infty}^{\infty}\int_{-\infty}^{\infty} \frac{1}{\pi N_o} \exp\left\{-\frac{||\underline{m} + \underline{\alpha}||^2 + ||\underline{\alpha}||^2}{N_o}\right\} d\underline{\alpha}$$

$$= \frac{1}{2} \exp\left\{-\frac{||\underline{m}||^2}{2N_o}\right\} \quad , \tag{148}$$

or

$$P_e = \frac{1}{2} \exp\left\{-\frac{PT}{2N_o}\right\} \quad . \tag{149}$$

Although this expression is derived for FSK signals, it applies in general for noncoherent detection of binary orthogonal signals.

With nonlinear clipping, we can follow arguments similar to the earlier results to get an error probability

$$P_e = \frac{1}{2} \exp\left\{-\frac{PT}{2N_o'}\right\} \quad , \tag{150}$$

where N_o' satisfies

$$N_o'W = \frac{1}{2}\overline{c^2} \quad , \tag{151}$$

or, in terms of basic parameters,

$$N_o' = N_o\left\{1 - \Phi(D) + \beta^2\left(\frac{P}{N_o W}\right)\Phi(E)\right\} \quad , \tag{152}$$

where D and E are given in Eqs. (136) and (137). Equation (150) is plotted for various parameters in Fig. 20.

C. Binary Phase-Shift Keying (PSK)

Although PSK is not commonly used at VLF/LF, we present it here because it is similar to the minimum-shift-keying (MSK) scheme now planned for several new VLF/LF systems. For binary PSK, the two signals are

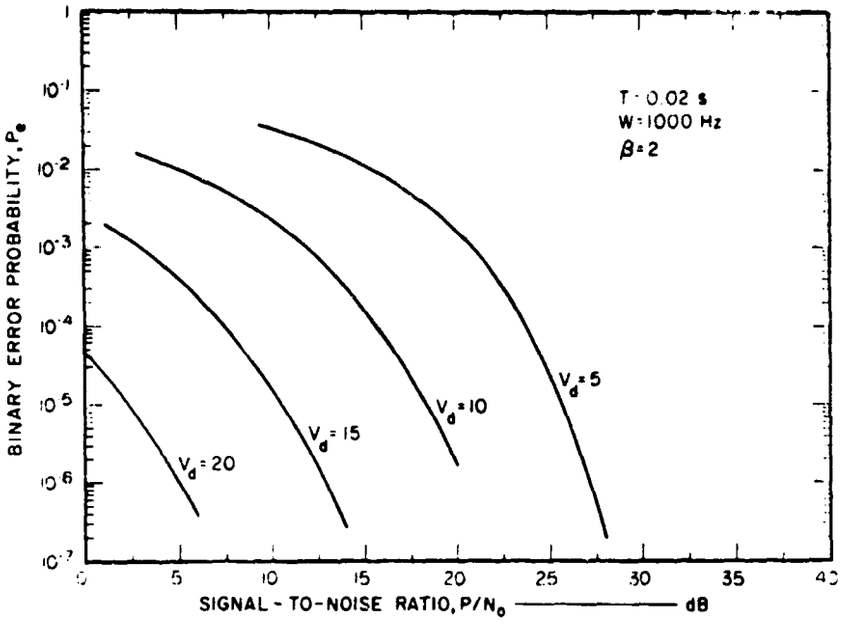

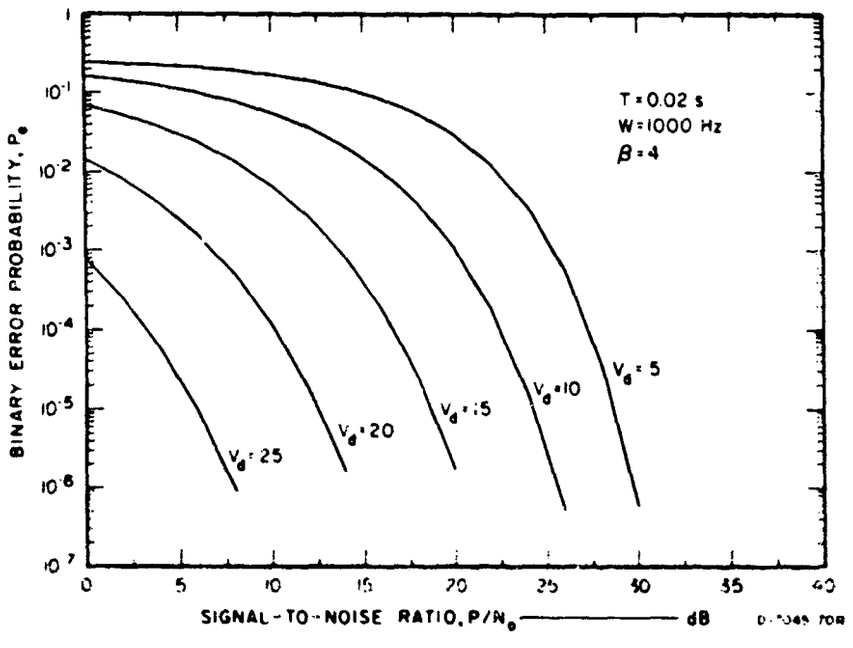

FIGURE 20 BINARY ERROR PROBABILITY FOR NONCOHERENT FSK—CLIPPING

$$m_1(t) = \sqrt{2P}\sin\omega_o t \qquad \text{for Mark}$$

$$m_o(t) = -\sqrt{2P}\sin\omega_o t \qquad \text{for Space} \quad . \tag{153}$$

Note that for this signal set we have simply

$$\rho = -1 \quad . \tag{154}$$

Coherent detection without any nonlinear clipping is simply represented in the receiver of Fig. 10, and the error probability is given by Eq. (93) with $\rho = -1$ and $\overline{c^2} = A^2 e^{2\sigma_n^2}$. Hence,

$$P_e = \Phi\left(\sqrt{\frac{2PT}{N_o}}\right) \quad . \tag{155}$$

Since

$$A^2 e^{2\sigma_n^2} = 2N_o W \quad . \tag{156}$$

We plot this curve in Fig. 21 where

$$\left(\frac{P}{N_o}\right)_{db} = 10\log_{10}\left(\frac{P}{N_o}\right) \quad . \tag{157}$$

With clipping in the front end, we have from Eq. (93) with $\rho = -1$,

$$P_e = \tfrac{1}{2}\left(\sqrt{\frac{4PWT}{\overline{c^2}}}\right) \quad , \tag{158}$$

where, as before,

$$\overline{c^2} = A^2 e^{2\sigma_n^2}\left\{1 - \tfrac{1}{2}\left(\frac{\log_e(B/A) - 2\sigma_n^2}{\sqrt{2\sigma_n^2}}\right)\right\} + B^2\,\tfrac{1}{2}\left(\frac{\log_e(B/A)}{\sqrt{2\sigma_n^2}}\right) \quad . \tag{159}$$

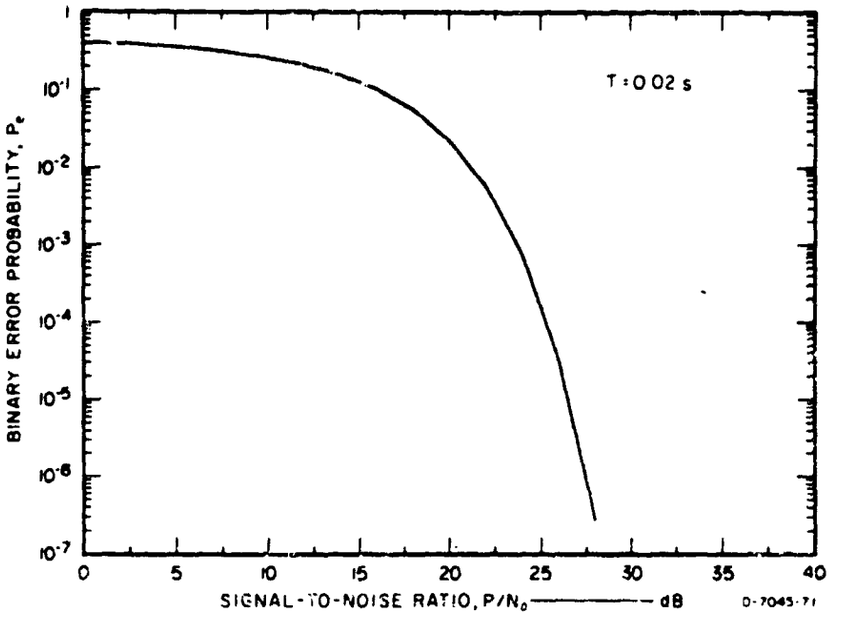

FIGURE 21 BINARY ERROR PROBABILITY FOR COHERENT FSK—NO CLIPPING

Again, choosing the clipping level,

$$B = \beta\sqrt{2P} \tag{160}$$

we can write P_e in terms of parameters P, N_o, β, V_d, T, and W,

$$P_e = \frac{1}{2}\left(\left[\frac{2PT}{N_o\left[1 - \frac{1}{2}(D) + \beta^2\left(\frac{P}{N_o W}\right)\frac{1}{2}(E)\right]}\right]^{\frac{1}{2}}\right) , \tag{161}$$

where D and E are defined in Eqs. (136) and (137).

Noncoherent detection of PSK signals does not exist, except perhaps with a phase reference signal. Suppose, for example, beside the Mark-Space signals we have a reference signal given by

$$q(t) \quad \sqrt{2P}\sin\omega_o t \quad , \tag{162}$$

which is first transmitted during time [-T,0]. Then, during time interval [-T,0],

$$r'(t) = \sqrt{2P}\,\sin(\omega_o t + \theta) + n'(t) \qquad t\in[-T,0] \tag{163}$$

is received, while during [0,T],

$$\begin{aligned} r(t) &= \sqrt{2P}\,\sin(\omega_o t + \theta) + n(t) \qquad \text{for Mark} \\ r(t) &= -\sqrt{2P}\,\sin(\omega_o t + \theta) + n(t) \qquad \text{for Space} \end{aligned} \tag{164}$$

is received.

The situation is equivalent to receiving a total signal

$$r_T(t) = \begin{cases} r'(t) & t\in[-T,0] \\ r(t) & t\in[0,T] \end{cases} \tag{165}$$

in [-T,T] on which to base a decision on whether a Mark or a Space has been sent. Defining signals

$$m_1^T(t) = \begin{cases} q(t) & t\in[-T,0] \\ m_1(t) & t\in[0,T] \end{cases} \tag{166}$$

and

$$m_o^T(t) = \begin{cases} q(t) & t\in[-T,0] \\ m_o(t) & t\in[0,T] \end{cases}, \tag{167}$$

we have

$$\int_{-T}^{T} m_1^T(t)m_o^T(t)dt = \int_{-T}^{o} q^2(t)dt + \int_{0}^{T} m_o(t)m_1(t)dt \qquad (168)$$

$$= PT - PT$$

$$= 0 \quad .$$

We have the situation where two orthogonal signals are transmitted over [-T,T] with a random phase θ. Noncoherent detection of such signals is precisely the same as noncoherent detection of FSK signals (orthogonal signals) of total duration 2T. Hence, from Eq. (149), we have

$$P_e = \frac{1}{2} \exp\left(-\frac{PT}{N_o}\right) \qquad (169)$$

for noncoherent detection of PSK signals with a reference signal as stated above. For the case with clipping we have, from the results of FSK, the error probability

$$P_e = \frac{1}{2} \exp\left(-\frac{PT}{N_o'}\right) \quad , \qquad (170)$$

where

$$N_o' = N_o\left(1 - \tfrac{1}{4}(D) + \beta^2\left(\frac{P}{N_o W}\right)\tfrac{1}{4}(E)\right) \quad . \qquad (171)$$

The most common reference signal is the previously transmitted Mark or Space signal. This means that each transmitted signal is modulated relative to the previously transmitted signal. This efficient mode of noncoherent operation, called differential-phase shift keying (DPSK), results in the binary error probabilities given above.

D. Binary Minimum-Shift Keying (MSK)

Minimum shift keying is a patented scheme developed by the Collins Radio Company. This modulation scheme gives a signal in the channel that looks like FSK with a modulation index of m = 1/2. Normally FSK modulation with m = 1/2 would require discontinuous phase changes, which would be difficult for VLF/LF transmitters to handle. The MSK scheme gives continuous phase and an improved performance equivalent to that of PSK modulation.

Consider a basic information source that generates a Mark or Space once every T seconds. This binary information sequence is alternatively used to modulate two PSK modulators that are $\pi/2$ radians out of phase with each other. This results in two PSK signal sequences where phase changes occur at odd times (T, 3T, 5T, ...) in one and at even times (0, 2T, 4T, ...) in the other. The two PSK signals are amplitude modulated by $\sqrt{2P}\sin\omega_1 t$ and $\sqrt{2P}\cos\omega_1 t$, respectively, and summed before transmission. See Fig. 22, where $\omega_1 = \pi/2T$,

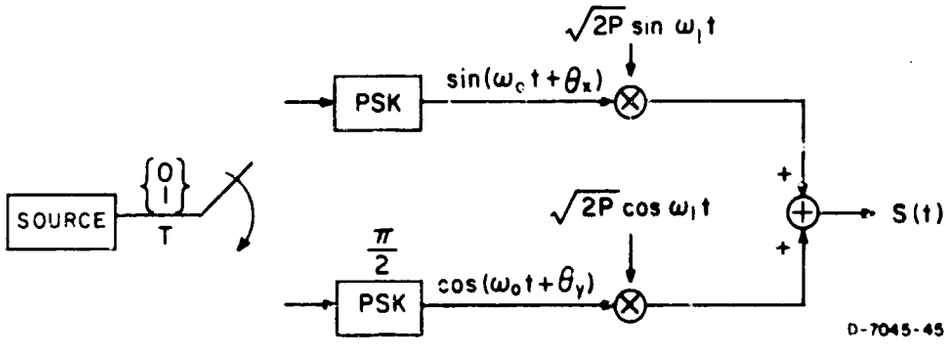

FIGURE 22 MSK MODULATOR REPRESENTATION

$$S(t) = \sqrt{2P}\left[\sin\omega_1 t\,\sin(\omega_0 t + \theta_x) + \cos\omega_1 t\,\cos(\omega_0 t + \theta_y)\right]$$

$$\theta_x = \begin{cases} 0 \\ \pi \end{cases} \quad \text{changes at T, 3T, 5T, ...} \tag{172}$$

$$\theta_y = \begin{cases} 0 \\ \pi \end{cases} \quad \text{changes at 0, 2T, 4T, ...} \quad .$$

The signal S(t) shown above appears as a continuous phase FSK signal with a modulation index of m = 1/2. Coherent detection is accomplished by separating the signal plus noise into two separate PSK-like signal-plus-noise sequences which are detected separately as shown in Fig. 23, where

$$\phi_s(t) = \sqrt{\frac{2}{T}} \sin \omega_1 t \sin \omega_o t$$
$$\phi_c(t) = \sqrt{\frac{2}{T}} \cos \omega_1 t \cos \omega_o t \qquad (173)$$

and

$$\int_0^{2T} \phi_s(t)\,\phi_c(t)\,dt = 0$$
$$\int_T^{3T} \phi_s(t)\,\phi_c(t)\,dt = 0 \qquad (174)$$

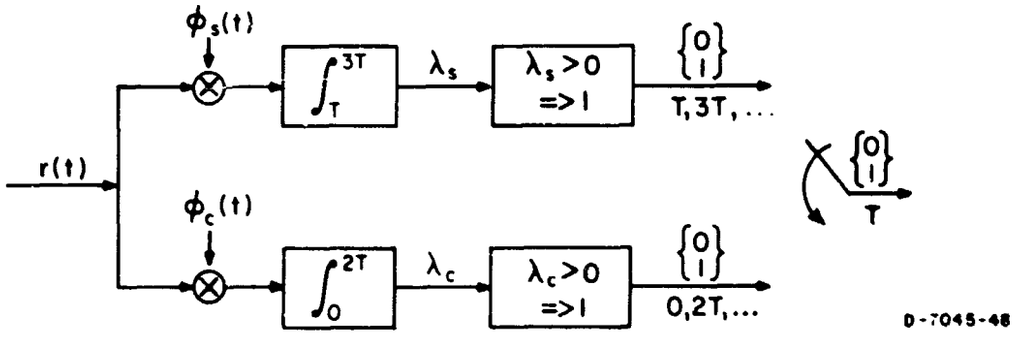

FIGURE 23 COHERENT MSK DETECTOR—NO CLIPPING

Since each side of the detector is essentially a PSK detector, the performance is that of coherent PSK detection with average power 1/2 P and signal duration 2T which results in total signal energy PT per transmitted Mark or Space. Hence, for each transmitted bit, the error probability for this coherent detector is

$$P_e = \Phi\left(-\sqrt{\frac{2PT}{N_o}}\right) \tag{175}$$

when no clipping is employed. This is plotted in Fig. 24 for T = 0.02.

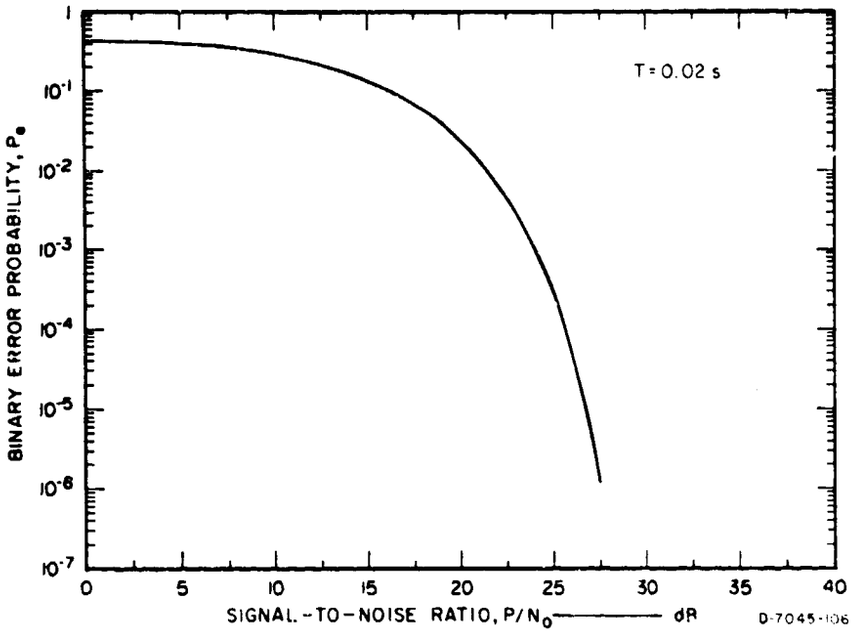

FIGURE 24 BINARY ERROR PROBABILITY FOR COHERENT MSK—NO CLIPPING

With clipping we have

$$P_e = \Phi\left(\left[\frac{2PT}{N_o\left|1 - \Phi(D) + \beta^2\left(\frac{P}{N_o W}\right)\Phi(E)\right|}\right]^{\frac{1}{2}}\right) , \tag{176}$$

just as in normal PSK signaling schemes. These probabilities are plotted in Fig. 25.

We were able to treat each side of the detector separately because of the orthogonality property of $e_s(t)$ and $e_c(t)$ shown in Eq. (174) and the fact that we have exact knowledge of the signal phase. We consider

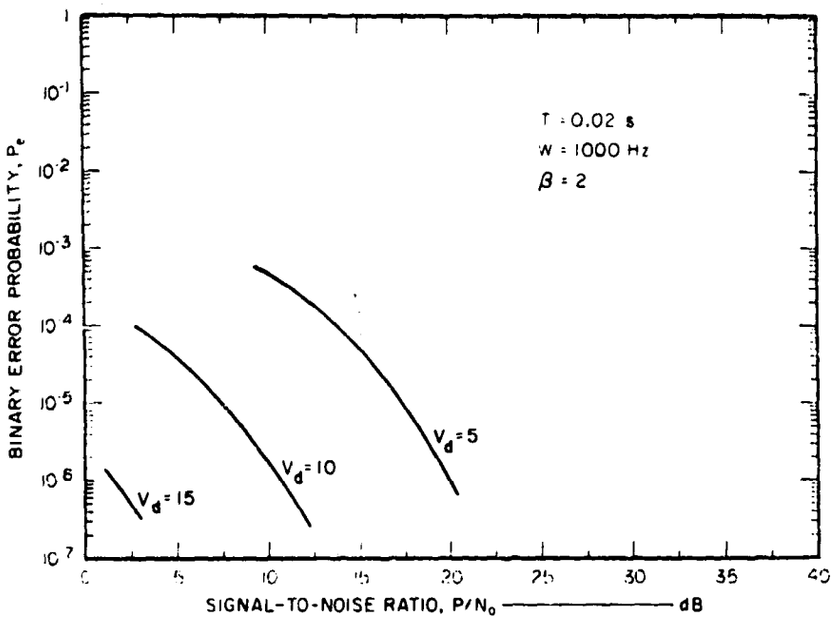

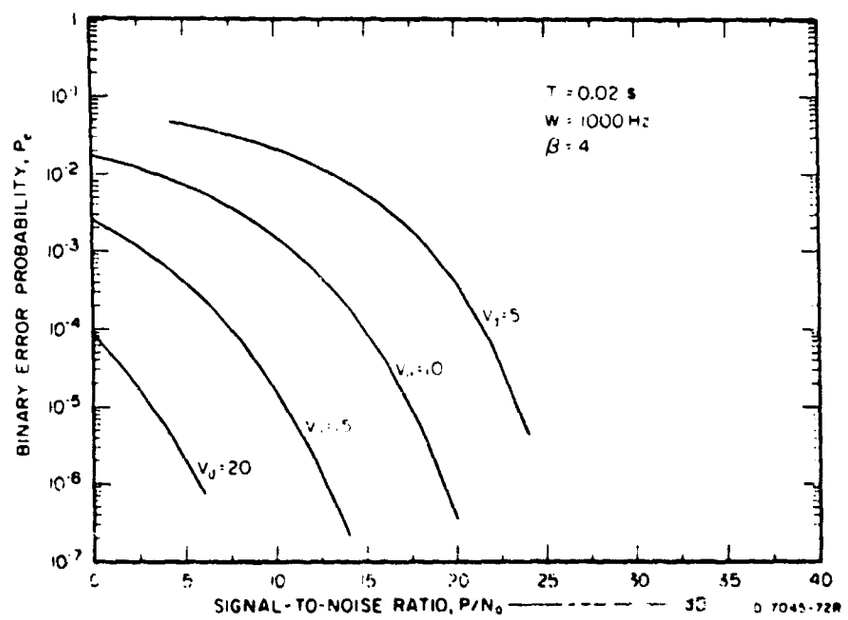

FIGURE 25 BINARY ERROR PROBABILITY FOR MSK—CLIPPING

now the difficult problem of operating in a differential mode similar to differential phase shift keying.

Suppose we have a reference signal

$$q(t) = \sqrt{2P}\left\{\sin \omega_1 t \sin \omega_o t + \cos \omega_1 t \cos(\omega_o t + \theta'_y)\right\} \qquad (177)$$

which is transmitted during [-T,T] and received as

$$r'(t) = \sqrt{2P}\left\{\sin \omega_1 t \sin(\omega_o t - \vartheta) + \cos \omega_1 t \cos(\omega_o t + \theta'_y - \vartheta)\right\} + n'(t) \qquad (178)$$

Defining

$$\begin{aligned}
\phi_{ss}(t) &= \sqrt{\frac{2}{T}} \sin \omega_1 t \sin \omega_o t \\
\phi_{sc}(t) &= \sqrt{\frac{2}{T}} \sin \omega_1 t \cos \omega_o t \\
\phi_{cs}(t) &= \sqrt{\frac{2}{T}} \cos \omega_1 t \sin \omega_o t \\
\phi_{cc}(t) &= \sqrt{\frac{2}{T}} \cos \omega_1 t \cos \omega_o t \quad ,
\end{aligned} \qquad (179)$$

we now consider how uncertainty in the phase of the transmitted signal can cause some mutual interference between the two PSK sides of the detector. Consider

$$\begin{aligned}
r'_s &= \int_{-T}^{T} r'(t)\phi_{ss}(t)\, dt \qquad (180) \\
&= \int_{-T}^{T} 2\sqrt{\frac{P}{T}} \sin^2 \omega_1 t \sin\left[\omega_o t - \theta\right] \sin \omega_o t\, dt \\
&+ \int_{-T}^{T} 2\sqrt{\frac{P}{T}} \sin \omega_1 t \cos \omega_1 t \cos\left[\omega_o t + \theta'_y - \vartheta\right] \sin \omega_o t\, dt \\
&+ n'_s \quad .
\end{aligned}$$

But

$$2\sqrt{\frac{P}{T}}\int_{-T}^{T}\sin^2\omega_1 t\,\sin\left[\omega_o t-\theta\right]\sin\omega_o t\,dt = \sqrt{PT}\cos\theta \quad , \tag{181}$$

and

$$2\sqrt{\frac{P}{T}}\int_{-T}^{T}\sin\omega_1 t\cos\omega_1 t\cos\left[\omega_o t+\theta_y'-\theta\right]\sin\omega_o t\,dt$$

$$=\frac{1}{2}\sqrt{\frac{P}{T}}\int_{-T}^{T}\sin 2\omega_1 t\,\sin\theta\,\sin\theta_y'\,dt$$

$$=\begin{cases} 0 & \theta_y' = 0 \text{ in } [-2T,2T] \\ & \theta_y' = \pi \text{ in } [-2T,2T] \\ \frac{2}{\pi}\sqrt{PT}\sin\theta & \theta_y' = 0 \text{ in } [-2T,0],\ \theta_y' = \pi \text{ in } [0,2T] \\ -\frac{2}{\pi}\sqrt{PT}\sin\theta & \theta_y' = \pi \text{ in } [-2T,0],\ \theta_y' = 0 \text{ in } [0,2T] \end{cases} \quad . \tag{182}$$

In summary, we have

$$r_s' = \sqrt{PT}\cos\theta + n_s'$$

$$+\begin{cases} 0 & \theta_y' = 0 \text{ in } [-2T,2T] \\ & \theta_y' = \pi \text{ in } [-2T,2T] \\ \frac{2}{\pi}\sqrt{PT}\sin\theta & \theta_y' = 0 \text{ in } [-2T,0],\ \theta_y' = \pi \text{ in } [0,2T] \\ -\frac{2}{\pi}\sqrt{PT}\sin\theta & \theta_y' = \pi \text{ in } [-2T,0],\ \theta_y' = 0 \text{ in } [0,2T] \end{cases} \quad . \tag{183}$$

Similarly,

$$r_c' = -\sqrt{PT}\sin\theta + n_c'$$

$$+\begin{cases} 0 & \theta_y' = 0 \text{ in } [-2T,2T] \\ & \theta_y' = \pi \text{ in } [-2T,2T] \\ \frac{2}{\pi}\sqrt{PT}\cos\theta & \theta_y' = 0 \text{ in } [-2T,0],\ \theta_y' = \pi \text{ in } [0,2T] \\ -\frac{2}{\pi}\sqrt{PT}\cos\theta & \theta_y' = \pi \text{ in } [-2T,0],\ \theta_y' = 0 \text{ in } [0,2T] \end{cases} \quad . \quad (184)$$

Here n_s' and n_c' are independent zero-mean Gaussian random variables with variance $N_o/2$. Defining the random variable that takes on one of three values with the following probabilities,

$$\delta = \begin{cases} -1 & p = \frac{1}{4} \\ 0 & p = \frac{1}{2} \\ 1 & p = \frac{1}{4} \end{cases} \quad , \quad (185)$$

we can represent the sine and cosine components of our reference signal as

$$\begin{aligned} r_s' &= \sqrt{PT}\cos\theta + n_s' + \frac{2\delta}{\pi}\sqrt{PT}\sin\theta \\ r_c' &= -\sqrt{PT}\sin\theta + n_c' + \frac{2\delta}{\pi}\sqrt{PT}\cos\theta \quad . \end{aligned} \quad (186)$$

This shows that, besides the noise terms n_s' and n_c', the reference signal can be corrupted by a strong interference term due to the signals in the other half of the detector. This means that using MSK on a bit-by-bit differential mode is impractical. We shall see, however, that taking a long stream of such channel bits (chips) to form a reference for another long stream of bits (or chips) can result in good performance.

Suppose that we now take N binary MSK channel bits or chips to transmit a single Mark or Space. This can be accomplished, for example by transmitting a pseudo-random binary sequence of chips for Mark and its negative for Space. Assume that we take N pseudo-randomly generated binary MSK chips to transmit a Mark or Space, and suppose that the N bits of the previously transmitted Mark or Space are used as a phase reference. This means that we have a noncoherent differential mode of operation on N chips, similar to the differential PSK scheme described earlier.

Collecting the N sine and cosine components of our previously transmitted signal, we have

$$R'_s = \sum_{k=1}^{N} r'_s(k)$$

$$= N\sqrt{PT}\cos\theta + \sum_{k=1}^{N} n'_s(k) \qquad (187)$$

$$+ \frac{2}{\pi}\sqrt{PT}\sin\theta \sum_{k=1}^{N} \delta_k$$

and

$$R'_c = \sum_{k=1}^{N} r'_c(k)$$

$$= -N\sqrt{PT}\sin\theta + \sum_{k=1}^{N} n'_c(k) \qquad (188)$$

$$+ \frac{2}{\pi}\sqrt{PT}\sin\theta \sum_{k=1}^{N} \delta_k \quad ,$$

as the sine and cosine components of our reference sequence where the index k corresponds to the k^{th} chip in the reference sequence. The terms

$$N_c' = \sum_{k=1}^{N} n_c'(k) \tag{189}$$

and

$$N_s' = \sum_{k=1}^{N} n_s'(k) \tag{190}$$

are independent zero-mean Gaussian random variables with variance $NN_o/2$. Assuming that chip sequences are pseudo-randomly generated, we can take the random variables $\{\delta_k\}_{k=1}^{N}$ to be independent, so that the sequence

$$D' = \sum_{k=1}^{N} \delta_k \tag{191}$$

approaches a Gaussian random variable in distribution as N gets large. The sine and cosine components of the reference signal are thus

$$\begin{aligned} R_s' &= N\sqrt{PT}\cos\theta + N_s' + \frac{2}{\pi}\sqrt{PT}\sin\theta\, D' \\ R_c' &= -N\sqrt{PT}\sin\theta + N_c' + \frac{2}{\pi}\sqrt{PT}\cos\theta\, D' \quad , \end{aligned} \tag{192}$$

where N_s', N_c', and D' are independent zero-mean Gaussian random variables (D' being assumed to be Gaussian) with variances

$$\begin{aligned} \overline{N_s'^2} &= \overline{N_c'^2} = NN_o/2 \\ \overline{D^2} &= N/2 \quad . \end{aligned} \tag{193}$$

Note that the noise components due to the interference,

$$\begin{aligned} &\frac{2}{\pi}\sqrt{PT}\sin\vartheta\, D' \quad , \\ &\frac{2}{\pi}\sqrt{PT}\cos\vartheta\, D' \quad , \end{aligned} \tag{194}$$

form a vector that is orthogonal to the signal vector formed by

$$N\sqrt{PT}\cos\theta \quad , \qquad -N\sqrt{PT}\sin\theta \quad . \tag{195}$$

This means that, since noise that is orthogonal to the signal vector can only cause errors, the noise term due to interference is equivalent to a noise vector having equal energy in all directions of energy,

$$\frac{2}{\pi} PT\ N \tag{196}$$

in any given direction. A similar argument applies to the transmitted signal. Hence the differential MSK sequence of length N performs like a differential PSK scheme with signal energy

$$N^2\ PT \tag{197}$$

and noise spectral density

$$N\left(\frac{N_o}{2} + \frac{PT}{\pi^2}\right) \quad . \tag{198}$$

The error probability is thus

$$P_e = \frac{1}{2}\exp\left\{-N\left(\frac{PT}{N_o + \frac{2PT}{\pi^2}}\right)\right\} \tag{199}$$

or

$$P_e = \frac{1}{2}\exp\left\{-N\left(\frac{\pi^2 PT}{\pi^2 N_o + 2PT}\right)\right\} \quad . \tag{200}$$

This expression, which assumes that no clipping has occurred, is plotted in Fig. 26. With clipping we have

$$P_e \quad \frac{1}{2}\exp\left\{-N\left(\frac{\pi^2 PT}{\pi^2 N_o' + 2PT}\right)\right\} \quad , \tag{201}$$

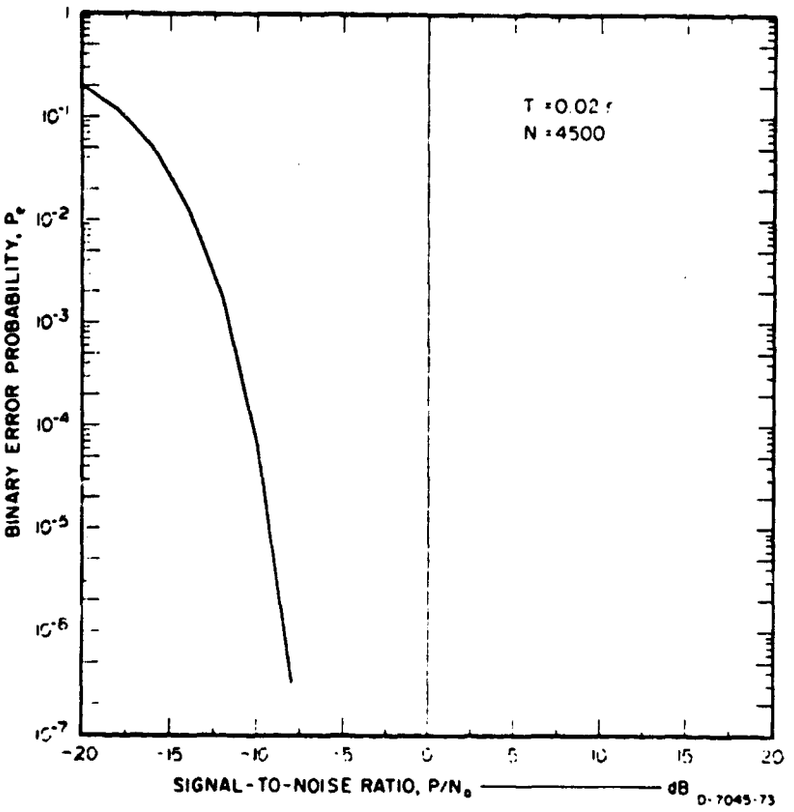

FIGURE 26 BINARY ERROR PROBABILITY FOR DIFFERENTIAL MSK

where, as before,

$$N_o' = N_o\left\{1 - \Phi(D) + \beta^2\left(\frac{P}{N_o W}\right)\Phi(E)\right\} \quad . \tag{202}$$

E. M-ary Minimum Shift Keying

We now consider schemes that take N binary MSK chips to transmit one of M messages. In general, the performance of these schemes is difficult to evaluate, so we must resort to finding upper bounds on the error probabilities. In this section, we restrict ourselves to two M-ary signal schemes, coherent orthogonal signals, and coherent pseudo-randomly generated signals.

Suppose that the M signals consisting of a sequence of binary MSK chips are represented by

$$s_i(t) = \sum_{j=0}^{N-1} s_{ij} p(t - jT) \qquad t \in [0,NT] \qquad i = 1, \ldots, M \quad , \tag{203}$$

where

$$s_{ij} = \begin{cases} 1 \\ -1 \end{cases}, \text{ and}$$

$p(t)$ is a pulse of duration T and energy PT.

Also, let

$$r(t) \qquad t \in [0,NT]$$

be the received signal which consists of the transmitted signal plus additive atmospheric noise with spectral density $N_o/2$ as before. Defining

$$||f||^2 = \int_0^{NT} f^2(t)\, dt \tag{204}$$

for any time function f(1) over [0,NT], we consider events

$$\mathcal{E}_{ik} = \left\{ ||r - s_k||^2 < ||r - s_i||^2 \,\middle|\, s_i \text{ is sent} \right\} \tag{205}$$

for i, k = 1, 2, ..., M. If the i^{th} signal is transmitted and an optimum white Gaussian noise receiver is used (as in the case of interest), the k^{th} signal is mistakenly assumed to have been sent by the receiver when the event $\mathcal{E}_{ik}$ occurs. This event occurs with probability

$$\begin{aligned} P_r\{\mathcal{E}_{ik}\} &= P_r\left\{ n > \frac{||s_k - s_i||}{2} \right\} \\ &= \tfrac{1}{2}\left(\frac{||s_k - s_i||}{\sqrt{2N_o}} \right) \quad . \end{aligned} \tag{206}$$

In general, when the i^{th} signal is transmitted, an error occurs if one or more of the events

$$\mathcal{E}_{ik} \qquad k = 1, 2, \ldots, M \quad ; \quad k \neq i \tag{207}$$

occurs. Hence, the error probability when the i^{th} signal is transmitted is given by

$$P_r\{\mathcal{E}|s_i \text{ is sent}\} = P_r\left\{\bigcup_{\substack{k=1 \\ k\neq i}}^{M} \mathcal{E}_{ik}\right\} \quad . \tag{208}$$

A well-known property of probabilities is that the probability of a union of events is less than the sum of the probabilities of each event. Hence, we have a bound

$$P_r\{\mathcal{E}|s_i \text{ is sent}\} \leq \sum_{\substack{k=1 \\ k\neq i}}^{M} P_r\{\mathcal{E}_{ik}\} \tag{209}$$

or

$$P_r\{\mathcal{E}|s_i \text{ is sent}\} \leq \sum_{\substack{k=1 \\ k\neq i}}^{M} \Phi\left(\frac{||s_k - s_i||}{\sqrt{2N_o}}\right) \quad . \tag{210}$$

When there is an orthogonal signal set, then

$$\int_0^{NT} s_i(t)s_k(t)\,dt = 0 \qquad k \neq i \tag{211}$$

and

$$||s_i - s_k||^2 = 2NPT \qquad k \neq i \quad . \tag{212}$$

Thus, for the orthogonal signal set, we have

$$P_r\{\mathcal{E}|s_i \text{ is sent}\} \leq \sum_{\substack{k=1 \\ k\neq i}}^{M} \Phi\left(\sqrt{\frac{NPT}{N_o}}\right) \tag{213}$$

or

$$P_r\{\mathcal{E}|s_i \text{ is sent}\} < M\,\Phi\left(\sqrt{\frac{NPT}{N_o}}\right) \quad . \tag{214}$$

Since this bound does not depend on which signal is sent, the error probability when any signal is sent has the same bound. The probability of error, P_e, when any signal is sent is thus bounded by,

$$P_e < M\,\Phi\left(\sqrt{\frac{NPT}{N_o}}\right) \quad , \tag{215}$$

which is plotted in Fig. 27.

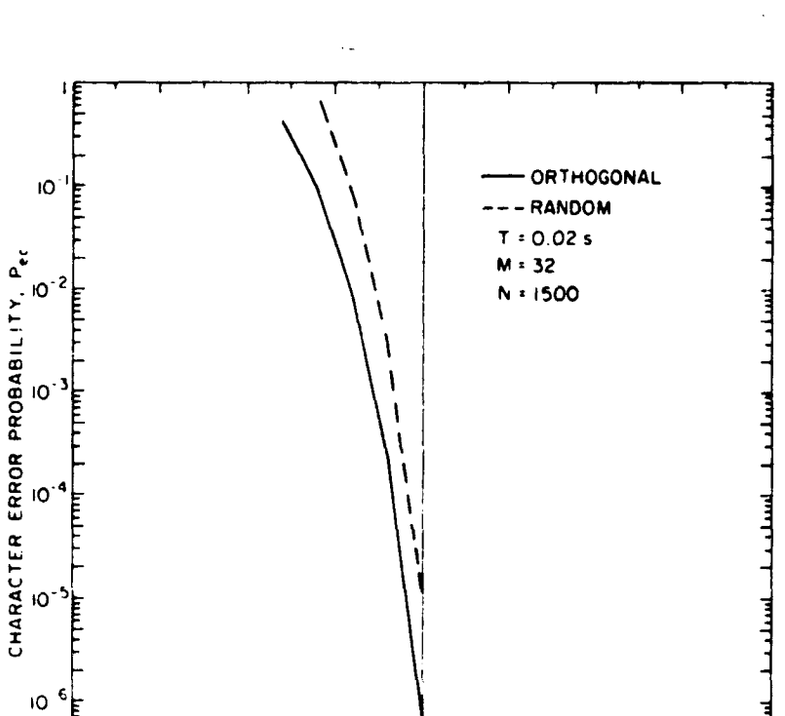

FIGURE 27 CHARACTER ERROR PROBABILITY OF MSK SEQUENCES

When the signals are not orthogonal but are generated pseudo-randomly by independent pseudo-random-sequence generators, Eq. (213) still applies. Hence, when the i^{th} signal is sent, the error probability is bounded by

$$P_r\{\mathcal{E}|s_i \text{ is sent}\} \leq \sum_{\substack{k=1 \\ k\neq i}}^{M} \Phi\left(\frac{||s_k - s_i||}{\sqrt{2N_o}}\right) \quad . \tag{216}$$

In general, we are interested not in the performance of a given pseudo-randomly generated signal set but in the average performance when a large class of such signal sets are used. Hence, when s_i is sent, we are interested in the average error probability where we average over the whole ensemble of pseudo-randomly generated signal sets. Taking averages of Eq. (216) we have,

$$\overline{P_r\{\mathcal{E}|s_i \text{ is sent}\}} \leq \sum_{\substack{k=1 \\ k\neq i}}^{M} \overline{\Phi\left(\frac{||s_k - s_i||}{\sqrt{2N_o}}\right)} \quad . \tag{217}$$

The error function has a bound

$$\Phi(x) < \exp\left\{-\frac{x^2}{2}\right\} \quad , \tag{218}$$

so that Eq. (217) can be further bounded by

$$\overline{P_r\{\mathcal{E}|s_i \text{ is sent}\}} < \sum_{\substack{k=1 \\ k\neq i}}^{M} \overline{\exp\left\{-\frac{||s_k - s_i||^2}{4N_o}\right\}} \quad . \tag{219}$$

Note that

$$\begin{aligned} ||s_k - s_i||^2 &= \int_0^{NT} \left[s_k(t) - s_i(t)\right]^2 dt \\ &= PT \sum_{j=0}^{N-1} \left[s_{kj} - s_{ij}\right]^2 \quad . \end{aligned} \tag{220}$$

Thus

$$\overline{\exp\left\{-\frac{||s_k - s_i||^2}{4N_o}\right\}} = \overline{\prod_{j=0}^{N-1} \exp\left\{-\frac{PT}{4N_o}(s_{kj} - s_{ij})^2\right\}} \quad . \tag{221}$$

We assume that the ensemble of signal sets is generated in such a manner that the components of any signal are essentially independent of each other and of other signal components and take on either +1 or -1 with equal probability. Hence,

$$\overline{\prod_{j=0}^{N-1} \exp\left\{-\frac{PT}{4N_o}\left(s_{kj} - s_{ij}\right)^2\right\}} = \left[\overline{\exp\left\{-\frac{PT}{4N_o}\left(s_{kj} - s_{ij}\right)^2\right\}}\right]^N$$

$$= \left[\frac{1}{2} + \frac{1}{2}\exp\left\{-\frac{PT}{N_o}\right\}\right]^N \quad . \tag{222}$$

The total probability of error, given that s_i is transmitted, is bounded by

$$P_r\left\{\mathcal{E} \mid s_i \text{ is sent}\right\} < \sum_{\substack{k=1 \\ k\neq i}}^{M} \left[\frac{1}{2} + \frac{1}{2}\exp\left\{-\frac{PT}{N_o}\right\}\right]^N \quad , \tag{223}$$

or

$$P_e < M\left[\frac{1}{2} + \frac{1}{2}\exp\left\{-\frac{PT}{N_o}\right\}\right]^N \tag{224}$$

is the bound on the probability that any signal transmitted gives an error. Equation (224) can be written in a more familiar form as,

$$P_e < M \exp\left\{-N \log_e\left(\frac{2}{1 + \exp\left(-\frac{PT}{N_o}\right)}\right)\right\} \quad . \tag{225}$$

This is plotted in Fig. 27.

In both Eq. (215) and Eq. (225), for the case of front end non-linear clipping, the term N_o is again replaced by

$$N_o' = N_o\left\{1 - \Phi(D) + \beta^2\left(\frac{P}{N_o W}\right)\Phi(E)\right\} \tag{226}$$

as before.

In the preceding derivation of the performance of typical equipment modems in the presence of atmospheric noise, improvement is shown to result from wideband clipping at the front end of the receiver. The development accounts for the reduction in impulsive noise by the clipper and hence predicts an improvement in signal-to-noise ratio in the stages of the receiver following the clipper. While the predicted improvement is valid when the clipping level is well above the rms noise level in the wideband portion of the receiver, when the noise clipper is active an appreciable fraction of the time these predictions become inaccurate. One reason for this inaccuracy is that account is not taken of the loss in signal energy as a result of the operation of the noise clipper.

An approximate correction may be made as follows:

let P_B = probability that the noise level exceeds the clipping level, B.

Then, during the time that the clipper is saturated by large noise pulses, no signal power is transmitted through the clipper, and the loss in signal power is given by:

$$\frac{P}{P'} = \frac{1}{1 - P_B}$$

All appropriate curves in this report include this correction.

VI CONCLUSION

We have computed the performance of several generic VLF/LF modulation-demodulation schemes, using the atmospheric noise model developed in Part One. In general, these calculations assume that the integration time T (baud time) is large enough so that the integrator output is Gaussian in distribution. When clipping is performed before integration, this assumption is even better. For the case of no clipping, this analysis results in classical white Gaussian noise error probabilities. With clipping, the detail properties of atmospheric noise become important, and such parameters as front-end bandwidth (W), clip level relative to signal peak (β), and noise voltage deviation (V_d) become important.

APPENDIX

Here we consider coherent PSK and MSK performance when the integration time T is small compared to the atmospheric noise correlation time and when no clipping is introduced. First consider the PSK signals

$$\begin{aligned} S_o(t) &= \sqrt{2P}\,\sin \omega_o t \qquad 0 \le t \le T \\ S_1(t) &= -\sqrt{2P}\,\sin \omega_o t \qquad 0 \le t \le T \quad . \end{aligned} \tag{227}$$

Suppose that the signal $S_o(t)$ is transmitted. The received signal is then

$$r(t) = A\, e^{n(t)} \cos\left[\omega_o t + \theta\right] + S_o(t) \quad . \tag{228}$$

The coherent receiver correlates the received signal with

$$\begin{aligned} \Delta S(t) &= S_o(t) - S_1(t) \\ &= 2\sqrt{2P}\,\sin \omega_o t \end{aligned} \tag{229}$$

to obtain the test statistics

$$\begin{aligned} \lambda &= \int_0^T r(t)\,\Delta S(t)\,dt \\ &= 2PT + 2\int_0^T A\, e^{n(t)} \cos\left[\omega_o t + \theta\right] \sqrt{2P}\,\sin \omega_o t\,dt \quad . \end{aligned} \tag{230}$$

The receiver bases its decision on λ in the following way:

$$\begin{aligned} &\text{If} \quad \lambda > 0 \quad , \quad \text{choose} \quad S_o \\ &\text{If} \quad \lambda \le 0 \quad , \quad \text{choose} \quad S_1 \quad . \end{aligned} \tag{231}$$

We now make the assumption that T is small enough so that n(t) and θ are essentially constant over the time interval [0,T]. Therefore

$$\lambda = 2PT + 2A\, e^{n} \sqrt{2P} \int_0^T \cos\left[\omega_o t + \theta\right] \sin \omega_o t \, dt \tag{232}$$

$$= 2PT + \sqrt{2P}\, A\, e^{n}\, T \sin \theta \quad .$$

An error occurs if $\lambda \leq 0$ when $S_o(t)$ is transmitted. Hence the error probability is

$$\begin{aligned} P_e &= P_r\left\{\lambda \leq 0 \,\middle|\, S_o \text{ is sent}\right\} \\ &= P_r\left\{2PT + \sqrt{2P}\, A\, e^{n}\, T \sin\theta \leq 0\right\} \\ &= P_r\left\{e^{n} \sin\theta \leq -\frac{\sqrt{2P}}{A}\right\} \quad . \end{aligned} \tag{233}$$

Since we assume that θ is completely unknown, we assume that it has uniform probability over $[0,2\pi]$. Consequently, its probability density is

$$P_\theta(\alpha) = \begin{cases} \frac{1}{2\pi} & 0 \leq \alpha \leq 2\pi \\ 0 & \text{elsewhere} \end{cases} \quad . \tag{234}$$

Since sin θ can be positive or negative with equal probability, by symmetry we have

$$P_e = P_r\left\{e^{n} \sin\theta \geq \frac{\sqrt{2P}}{A}\right\} \quad . \tag{235}$$

Clearly, when $\pi \leq \theta \leq 2\pi$,

$$e^{n} \sin\theta \geq \frac{\sqrt{2P}}{A} \tag{236}$$

$$P_e = \int_0^{\pi} P_r\left\{e^n \sin\theta > \frac{\sqrt{2P}}{A}\middle|\theta\right\} \frac{1}{2\pi}\, d\theta$$

$$= \frac{1}{2\pi} \int_0^{\pi} P_r\left\{e^n \geq \frac{\sqrt{2P}}{A \sin\theta}\middle|\theta\right\} d\theta \qquad (237)$$

$$= \frac{1}{2\pi} \int_0^{\pi} \Phi\left(\frac{\log_e\left(\frac{\sqrt{2P}}{A \sin\theta}\right)}{\sqrt{\sigma_n^2}}\right) d\theta \quad .$$

By symmetry we note that the same error probability applies when $S_1(t)$ is transmitted. Hence the total binary error probability for coherent binary PSK with integration time T smaller than the noise correlation time is given by

$$P_e = \frac{1}{2\pi} \int_0^{\pi} \Phi\left(\frac{\log_e\left(\frac{\sqrt{2P}}{A \sin\theta}\right)}{\sqrt{\sigma_n^2}}\right) d\theta \quad . \qquad (238)$$

This error probability is generally difficult to evaluate except by approximation and computer techniques. Coherent MSK also has this form for the probability of making a binary error.

REFERENCES

1. E. L. Younker, E. J. Baumann, J. K. Omura, and G. H. Price, "VLF/LF Communications during a Major Nuclear Attack (U)," Final Report, Contract DASA01-68-C-0013, SRI Project 7045, Stanford Research Institute, Menlo Park, California (in preparation), SECRET-RESTRICTED DATA.

2. E. T. Pierce, "The Thunderstorm as a Source of Atmospheric Noise at Frequencies between 1 and 100 kHz," Special Technical Report 2, Contract DASA01-68-C-0013, SRI Project 7045, Stanford Research Institute, Menlo Park, California (in preparation).

3. D. Middleton, Introduction to Statistical Communication Theory (McGraw-Hill Book Co., Inc., New York, New York, 1961).

4. K. Furutsu and T. Ishida, "On the Theory of Amplitude Distribution of Impulse Noise," J. Appl. Phys., Vol. 32, pp. 1206-1221 (July 1961).

5. B. A. Bowen, "Some Analytical Techniques for a Class of Non-Gaussian Processes," Research Rept. No. 63-3, Queen's University (June 1963).

6. J. Galejs, "Amplitude Distributions of Radio Noise at ELF and VLF," J. Geophys. Res., Vol. 71, pp. 201-216 (January 1966).

7. A. D. Watt and E. L. Maxwell, "Measured Statistical Characteristics of VLF Atmospheric Radio Noise," Proc. IRE, Vol. 45, pp. 55-62 (January 1957).

8. C. Clarke, P. A. Bradley, and D. E. Mortimer, "Characteristics of Atmospheric Radio Noise Observed at Singapore," Proc. IEE (London), Vol. 112, pp. 849-860 (May 1965).

9. W. Q. Crichlow, A. D. Spaulding, C. J. Roubique, and R. T. Disney, "Amplitude Probability Distributions for Atmospheric Radio Noise," NBS Monograph 23, National Bureau of Standards, Boulder, Colorado (1960).

10. O. Ibukun, "Structural Aspects of Atmospheric Radio Noise in the Tropics," Proc. IEEE, Vol. 54, pp. 361-367 (March 1966).

11. J. G. Kneuer, "A Simplified Physical Model for Amplitude Distribution of Impulsive Noise," IEEE Trans., Vol. COM-12, p. 220 (December 1964).

12. P. Beckmann, "Amplitude Probability Distribution of Atmospheric Radio Noise," Radio Science, Vol. 68D, pp. 723-736 (June 1964).

13. G. Foldes, "The Lognormal Distribution and Its Applications to Atmospheric Studies," Statistical Methods in Radio Wave Propagation, ed. W. C. Hoffman, pp. 227-232 (Pergamon Press, New York, New York, 1960).

14. T. Nakai, "The Study of Amplitude Probability Distribution of Atmospheric Radio Noise," Proc. Res. Inst. Atmos. (Japan), Vol. 7, pp. 12-17 (January 1960).

15. H. Hall, "A New Model for 'Impulsive' Phenomena: Application to Atmospheric-Noise Communication Channels," Ph.D. Thesis, Technical Report No. 7050-7, Stanford Electronics Laboratories, Stanford, California (August 1966).

16. R. M. Lerner, "Design of Signals," in Lectures on Communication System Theory, ed. E. J. Baghdady, pp. 243-277 (McGraw-Hill Book Co., Inc., New York, New York, 1961).

17. P. Mertz, "Model of Impulsive Noise for Data Transmission," IRE Trans. on Communications Systems, pp. 130-137 (June 1961).

18. P. Mertz, "Impulse Noise and Error Performance in Data Transmission," Memorandum RM-4526-PR, RAND Corporation, Santa Monica, California (April 1965).

19. International Radio Consultative Committee, "World Distribution and Characteristics of Atmospheric Radio Noise," International Telecommunication Union, Geneva (1964).

20. T. Nakai, "Calculated Statistical Characteristics of Atmospherics Radio Noise," Proc. Res. Inst. Atmos. (Japan), Vol. 10, pp. 13-24 (January 1963).

21. National Bureau of Standards, Handbook of Mathematical Functions, Applied Math. Series 55 (U S. Government Printing Office, Washington, D.C., 1964).

22. S. O. Rice, "Mathematical Analysis of Random Noise," Bell System Tech. J., Vols. 23 and 24 (1944, 1945).

23. M. S. Longuet-Higgins, "The Distribution of Intervals Between Zeroes of a Stationary Random Function," Phil. Trans. Roy. Soc. (London), Vol. 254, p. 557 (1962).

24. J. A. McFadden, "The Axis Crossing Intervals of Random Functions," IRE Trans., Vol. IT-2, pp. 146-150 (December 1956).

25. A. D. Watt, VLF Radio Engineering, International Series of Monographs in Electromagnetic Waves, Vol. 14 (Pergamon Press, New York, New York, 1967).

26. P. E. Bello, "Error Probabilities Due to Atmospheric Noise and Flat Fading in HF Ionospheric Communication Systems," IEEE Trans., Vol. COM-3, pp. 266-279 (September 1965).

27. J. I. Marcum, "Tables of the Q-Function," Report RM-339, RAND Corporation, Santa Monica, California (January 1950).

28. S. Stein and J. J. Jones, Modern Communication Principles (McGraw-Hill Book Co., Inc., New York, New York, 1967).

UNCLASSIFIED
Security Classification

DOCUMENT CONTROL DATA - R & D

Security classification of title, body of abstract and indexing annotation must be entered when the overall report is classified)

1. ORIGINATING ACTIVITY (Corporate author) Stanford Research Institute 333 Ravenswood Avenue Menlo Park, California 94025	2a. REPORT SECURITY CLASSIFICATION Unclassified 2b. GROUP N/A

3. REPORT TITLE

STATISTICAL ANALYSIS OF LF/VLF COMMUNICATION MODEMS

4. DESCRIPTIVE NOTES (Type of report and inclusive dates)
Special Technical Report 1

5. AUTHOR(S) (First name, middle initial, last name)
Jimmy K. Omura

6. REPORT DATE	7a. TOTAL NO. OF PAGES	7b. NO. OF REFS
August 1969	114	28

8a. CONTRACT OR GRANT NO	9a. ORIGINATOR'S REPORT NUMBER(S)
DASA01-68-C-0073 b. PROJECT NO. NWER Subtask HE 043	Special Technical Report 1 SRI Project 7045
c. d.	9b. OTHER REPORT NO(S) (Any other numbers that may be assigned this report) DASA-2324

10. DISTRIBUTION STATEMENT
This document is subject to special export controls and each transmittal to foreign governments or foreign nationals may be made only with prior approval of the Director, Defense Atomic Support Agency, Washington, D.C. 20305.

11. SUPPLEMENTARY NOTES	12. SPONSORING MILITARY ACTIVITY
	Director Defense Atomic Support Agency Washington, D.C. 20305

13. ABSTRACT

This is a two-part technical report that considers the short-time statistical modeling of atmospheric noise at VLF/LF frequencies and applies a new noise model to the performance evaluation of various generic VLF/LF communication modems. In Part One atmospheric noise is examined mainly from a statistical point of view. Next, various statistical models for this type of noise are examined; finally, a new model is developed and compared with available data. In Part Two this noise model is applied to the evaluation of the error probability calculations of various generic VLF/LF modems. Much of Part Two, particularly in regard to a receiver system employing no clipping, is based on classical white Gaussian noise analysis applied in generic modems of interest. When nonlinear clipping is applied, the detailed statistical behavior of atmospheric noise becomes more important, and results depend on the detailed structure of the noise.

DD FORM 1 NOV 65 1473 (PAGE 1)
S/N 0101-807-6801

UNCLASSIFIED
Security Classification

14 KEY WORDS	LINK A		LINK B		LINK C	
	ROLE	WT	ROLE	WT	ROLE	WT
Statistical analysis						
Very low frequency (VLF)						
Low frequency (LF)						
Communication system performance						
Binary error probability						
Communication modems						
On-off keying (CW)						
Frequency shift keying (FSK)						
Phase shift keying (PSK)						
Binary minimum shift keying (MSK)						
M-ary minimum shift keying						
Thunderstorm characteristics						
Short-time statistics of atmospheric noise						
Log-normal atmospheric noise model						